NUCLEAR SPACE POWER SYSTEM ANALYSES FOR THE UNMANNED MARS ROUND TRIP

PRINCETON UNIVERSITY

DEPARTMENT OF
AEROSPACE AND MECHANICAL SCIENCES

[redacted]

NUCLEAR SPACE POWER SYSTEM ANALYSES
FOR THE UNMANNED MARS ROUND TRIP

SUMMARY

An analysis was conducted to determine the best nuclear-turboelectric space powerplant to meet the requirements of an unmanned round-trip mission to Mars. The specific masses of both the Brayton cycle and liquid metal Rankine cycle were investigated for power levels from 500 kwe to 1500 kwe. Preliminary vehicle concepts were established and the specific masses of these spacecraft were then used to indicate the relative performance of the propulsion systems. The results of the analysis indicate that the 1500 kwe Brayton cycle space powerplant and its associated spacecraft can perform the selected mission better than the other configurations considered.

ACKNOWLEDGMENTS

The authors wish to express their gratitude for the continued support and encouragement associated with the Guggenheim Laboratories for the Aerospace Propulsion Sciences, Department of Aerospace and Mechanical Sciences, Princeton University.

Special thanks are extended to Mr. J. P. Layton who suggested the thesis topic and whose guidance and assistance were invaluable to its successful completion.

Mr. Peter M. Williams was extremely helpful in the reactor and shielding analyses as well as reviewing the text before printing. Dr. Morris Handelsman was particularly helpful in all matters concerning the mission analysis.

Many other members of the staff of the Guggenheim Laboratories contributed their time and efforts. Mr. Tony Poli and other members of the Drafting Group produced the drawings appearing in this thesis. Messrs. Lanny L. Hoffman and George A. Hazelrigg and members of the Computing Group aided in programming and running the digital computer programs. Miss Frances Allison typed the manuscript. The authors take this opportunity to thank them all.

Financial support of this research was provided by the National Aeronautics and Space Administration under Contract NASr-231.

TABLE OF CONTENTS

Page

TABLE OF CONTENTS (cont'd.)

TABLE OF CONTENTS (cont'd.)

LIST OF TABLES

LIST OF FIGURES

LIST OF FIGURES (cont'd.)

TABLE OF SYMBOLS

a = thrust acceleration, m/sec^2

B = radiator fin width, cm

B_c^2 = critical buckling

B_1 = radiator build-up factor

c_p = specific heat, kcal/kg ^oK

D = diameter, cm

E_2 = shielding integral

F = radiation view factor

f = fin effectiveness or thermal utilization

G = mass flow rate/unit area, kg/m^2sec

H = core length

h = specific enthalpy, kcal/kg

h_R = heat transfer coefficient, $kcal/m^2sec$ ^oK

J = integral of thrust acceleration, m/sec

k = thermal conductivity, kcal/hr m^2 ^oK

k_∞ = infinite multiplication factor

k_{eff} = effective multiplication factor

L = radiator tube length or diffusion length

M = mass, kg

N = number of tubes

TABLE OF SYMBOLS (cont'd)

P = power, kwe

p = pressure, kg/cm^2 , or resonance escape probability

Q = heat power, kcal /sec

R = orbit radius, A.U.

r = pressure ratio

S_v = radiation volume source strength, neutrons/cm^{2}sec

T = temperature, $^{\circ}$K

t = thickness, cm

V = characteristic velocity, km/sec

V_c = reactor core volume, cm^3

α = specific mass, kg/kwe

γ = ratio of specific heats

ϵ = emissivity or fast fission factor

η = efficiency

μ = viscosity

μ_a = linear attenuation coefficient

ν = number neutrons liberated/number neutrons absorbed

ρ = density, gm/cm^3

Σ_a = total absorption cross section

Σ_f = macrascopic fission cross section

TABLE OF SYMBOLS (cont'd)

Σ_r = macrascopic removal cross section

σ = Boltemann constant, 1.352×10^{-11} kcal/m^2sec $^oK^4$

σ_r = microscopic removal cross section

σ_s = microscopic scattering cross section

ϕ = radiation flux, mev/cm^2sec

Subscripts

c = compressor, cold, or center

f = final or fin

h = hot

g = generator

j = jet

o = initial

p = pump

PL = payload

pp = powerplant

R = radiator

s = spacecraft

sk = sink

T = transmitter

t = turbine or tube

w = wall

I. INTRODUCTION

The determination of man's relative biological position in the universe and the increased understanding of his environment in general are two of the primary motives for the National Space Program. The first major step in the exploration of our solar system will be realized in the near future with the landing of man on the moon. Although this feat is properly considered as representing vast scientific achievement, it will contribute only a small amount to satisfying man's curiosity about extraterrestrial life. Accordingly, the next logical phase in the space exploration program will be directed toward the exploration of the possible life supporting bodies in our solar system.

This thesis will treat one specific mission in this phase, the unmanned round-trip mission to Mars including the return of sizeable specimens of the Martian environment to low Earth orbit. A specific mission was chosen in order that realistic propulsion system parameters would be required in the study. The propulsion system requirements will receive the majority of the attention with the principal objective being to determine the best nuclear-turboelectric propulsion system suited to the mission. A nuclear propulsion system was selected because of the high energy requirement of the round trip mission to Mars.

Other nuclear propulsion schemes such as the nuclear rocket or nuclear-electric direct conversion could be used for this mission, but because of the size of the task this thesis is limited to nuclear-turboelectric systems.

The specific nuclear-turboelectric propulsion systems studied are the Rankine cycle powerplant and the Brayton cycle powerplant coupled to a magneto plasma dynamic are thruster. It is felt that these propulsion systems can be made available by the proposed time period of the mission, 1975-1985.

In the past, the two planets most often mentioned as being the first candidates for interplanetary exploration were Earth's nearest neighbors, Venus and Mars. Recently, however, the surface environment on Venus has been found to hold little chance of life supportance except in a narrow band. In fact the Mariner II flyby of 1962 found the surface in some areas to have a temperature on the order of 700°K and, in addition, very high winds and high dynamic pressures are probably present. (Reference 1). Mars thus appears to be the most promising planet to begin our search for extraterrestrial life.

Little is actually known about the body and surface of Mars. Several atmospheric models have been postulated from Earth-based observations and they tend to present a Martian environment that could conceivably be life supportant. Although

it is difficult to find exact agreement among the various models proposed, the concensus shows the atmosphere to consist primarily of nitrogen and carbon dioxide with argon and other gases in lesser amounts. The surface temperature is thought to vary in the neighborhood of $200^{o}K$ to $300^{o}K$ and the surface pressure from 10 to 100 mb. (References 2, 3). The basic atmospheric model should be greatly enhanced with the results of the Mariner Mars flyby in July 1965. This mission will attempt to analyze the Martian atmosphere as well as take pictures of the Martian surface with a resolution ten times greater than available from any Earth based telescope. (Reference 2).

Although the flyby missions of the Mariner class will certainly enhance our knowledge of the Martian surface and atmosphere, we will still be ignorant of the extent to which the important geological processes, as we know them on Earth, have taken place. To learn these things we must have accurate information about the physical characteristics of the planet.

To obtain this and other data, both the orbiter and soft-lander type missions are required. An orbiter would be capable of extensive photographic coverage as well as obtaining data on the gravity and magnetic fields, while a lander would be capable of accomplishing many geological and geophysical experiments such as pointed out in Reference 3.

Accordingly, the subsequent missions to the Mariner series will be those of Project Voyager with the first mission planned for 1971. (Reference 4). Voyager will initially consist of a 10,000 lb. spacecraft designed to study the Martian atmosphere, analyze its physical compositions and search for life on the Martian surface. It will contain a 2,000 lb. excursion vehicle for soft landing capabilities. Although no follow on programs to Project Voyager have been officially announced at present, several have been proposed. One of these, Project Beagle, would use a single Saturn V launch vehicle to land two 5,000 lb. laboratories on the planet and simultaneously orbit a 14,000 lb. payload. (Reference 5). Each lander would carry a variety of wet chemical and analytical experiments, similar to those used in Voyager, that would serve to analyze samples of the Martian surface.

A laboratory on the surface of Mars will undoubtedly provide much valuable information; however, it has one very serious limitation, its inability to analyze the unknown. The experiments performed in such a laboratory, no matter how complex, can look only for characteristics or physical phenomena with which we are familiar on Earth. This situation can be remedied in two ways: by landing man himself on Mars to run the analyses or by returning the samples to a manned Earth

orbiting laboratory. Thus, an unmanned round-trip mission to Mars with a sizeable amount of Martian environment returned to Earth orbit would seem to be the logical follow on mission to the soft landing laboratories. Because of the similarity to the manned mission, it is felt that the unmanned round-trip mission will also provide an actual flight test of prototype equipment and mission concepts for the first manned mission to Mars.

The largest factor upon which the success of such a mission depends is the proper selection of a suitable propulsion system. The two systems under investigation have been selected as the most likely nuclear-turboelectric systems to emerge within the desired time period of this mission. The liquid metal Rankine cycle has received the most attention in this country as far as development is concerned. (Reference 6). For this reason the liquid metal Rankine cycle developed in this analysis will draw heavily on these previously developed concepts and technology in hopes that it will represent the best that is predicted for the Rankine cycle technology in the time period of interest. For these reasons, the liquid metal Rankine cycle will often be referred to as the reference system in this analysis.

The Brayton cycle has received much interest in recent

years but very little actual development, particularly in the power range of interest. In this analysis, an investigation will be made to determine what the best of the Brayton cycle technology can offer in a space nuclear powerplant in the same time period.

The basic concepts and groundrules established for the development of a minimum mass nuclear electric space powerplant must necessarily depend on the characteristics of the specific mission to be accomplished. For this reason, the initial step in this analysis is to examine more closely the specific mission involved, namely, the unmanned round trip lander to Mars.

II. GENERAL REQUIREMENTS OF THE UNMANNED MARS ROUND TRIP MISSION

A. Mission Concept

In the chronological order of future space accomplishments, this mission would probably precede the first attempt at landing man on Mars. Because of the similarity in the mission profiles and the spacecraft propulsion systems required, many requirements of the unmanned mission would test the basic systems and procedures to be employed in the first manned mission.

The unmanned round trip mission to Mars should include the following phases: (1) spiral out from low earth orbit or boost to escape velocity, (2) heliocentric transfer to Mars, (3) spiral-in to low Mars orbit, (4) park in low Mars orbit while excursion vehicle departs, collects the specimens and returns, (5) spiral out from Mars, (6) heliocentric transfer to earth, and (7) spiral-in to a low earth orbit. There may well be some discussion as to where and how to examine the Martian specimens. For the time being it will be assumed that the specimens will be examined in a manned orbiting laboratory in low earth orbit. The subsequent rendezvousing procedures with a manned orbiting laboratory will not be covered here as it is assumed that this will be a routine practice by the time period of this mission. This final phase of the mission may have to be changed to deliver the samples to a low moon orbit or some

other place if the present concept proves impractical.

The planned time period based on a logical sequence of this mission in the national space program and on estimated equipment availability will be from 1975 to 1985. The mission itself will be limited to between one and two years duration. The shorter limitation of one year is considered to be a probable minimum time for this mission with the type of propulsion systems presently foreseen for this time period. The two year maximum limitation is likewise considered to be a practical reliability limit of the presently conceived hardware. More important, perhaps, is the factor of human endurance for the follow on manned missions to Mars.

As stated previously, the primary objective of this mission will be to return samples of the Mars surface to an Earth orbiting laboratory for analysis. In conjunction with this, a number of additional objectives of considerable importance to subsequent missions can be accomplished. Two examples are described below.

The first of these is the transmission of real time television back to Earth from the orbiting vehicle. The factor that would make this possible for the first time is the availability of the large electrical power supply need to transmit wide bandwidth data. The power is available from the

orbiting nuclear electric propulsion system. Another possibility is the use of high definition radar from the orbiting vehicle for range and surface mapping. Both of these schemes are covered in more detail in the following section.

The second additional mission will be that of checking out and proving the reliability of many of the actual subsystems that will be employed on the first manned mission to Mars. Of principal interest here will be the nuclear-electric propulsion system and the hardware employed for the descent, ascent and rendezvous phases from Mars orbit.

B. Payload

The total mass of the Martian samples, including their containers, to be returned to Earth orbit has been arbitrarily selected as 115 Kg. This would consist of a subsurface core sample, a quantity of scraped surface material, and a number of small samples which have been exposed to the Martian environment.

One type of mechanism which could collect these samples is described in Reference 7. It consists of a coring device, a surface scraper and sample cannisters. The cannisters themselves are used as coring pipe as well as storage for surface scrapings. When filled, they are stored back aboard the ascent

vehicle. No attempt has been made to design the actual device along these or any other lines; however, the concept, as presented in Reference 7, is considered highly feasible.

The total weight of the excursion vehicle, at separation from the parent spacecraft in parking orbit, is limited in Reference 7 to 9,115 kg. The vehicle itself is a lifting body of L/D approximately equal to one. Contained in this vehicle, along with the ascent vehicle, are such things as heat sheild, landing propulsion and parachutes, power supply, and communications and experimental equipment. The ascent vehicle, limited to 2,727 kg, contains the payload cannisters as well as the necessary propellant and electronics equipment to deliver the payload to the parent spacecraft parked in Mars orbit.

The details of the excursion vehicle are omitted herein as they are not essential to the primary objective of this thesis. The data presented in Reference 7, however, has been verified to the extent that the masses of the major components of the excursion vehicle are well within reason for this particular mission. They compare favorably, when properly scaled, with preliminary designs for the heavier manned excursion module using similar concepts such as presented in Reference 8. It is for these reasons that the drop off mass at Mars has been selected as 9,000 Kg. This is the total mass of the complete

excursion vehicle on its initial separation from the parent spacecraft minus the 115 Kg of sample to be returned to the spacecraft in Mars orbit. The altitude of the Mars orbit, for these calculations, is assumed to be the same as that of Reference 7, approximately 800 Km.

As mentioned previously, a secondary objective for the nuclear electric spacecraft could be that of real-time television coverage of the Martian surface. This would be accomplished from the parent spacecraft in parking orbit while awaiting the return of the excursion module. While in the parking orbit about Mars, the output of the nuclear electric power supply would be switched from propulsion purposes to that of microwave transmissions. From Reference 9, the vehicle transmitter power in kilowatts, P_T, the vehicle antenna diameter in feet, D_T, and the vehicle distance to Earth in astronautical units, R, are related by:

$$P_T D_T^2 = 560 R^2 \qquad (1)$$

Equation (1) is derived in Appendix B. With the high power levels available from a nuclear electric system, real time television coverage or other wide-band information can be transmitted from Mars to Earth with the use of comparatively small antennas. For a 20 kw output an antenna diameter of approximately seven feet would suffice.

It can be readily seen that the utilization of a nuclear electric propulsion system has several advantages for communications purposes. Since the power required for propulsion generally exceeds that required for microwave transmission, an additional savings in mass can be achieved if a portion of the radiator not required by the propulsion systems in the Mars orbit phase of the mission is designed to perform as an antenna as well as a heat radiator. Although there are many problems associated with an integrated design as such, the benefits to be gained in mass savings alone are great.

In Reference 9, the weight of the transmitter for television transmission from Mars is estimated at 341 kg. In a fully integrated system using the major component of a nuclear electric propulsion system, this would be the only major weight addition required to permit continuous television coverage while in a Martian orbit. Equipment for range and surface mapping might also be considered since the power requirements are similar to those for television transmissions.

Since the mass of the transmitter just considered is less than 4% of the previously selected dropoff mass at Mars, it will be neglected in the preliminary mission analysis. In the final mission analysis, however, the payload will be adjusted to allow for such equipment although no attempt will be made to define exactly what might be carried.

C. Effect of Propulsion System Parameters

As the initial step in selecting a propulsion system, a preliminary mission analysis was made to determine the relative effect of the propulsion system parameters on mission performance. The investigation was made to show the effect of the parameter's specific powerplant mass, α_s, electric thruster efficiency, η , and the power level, P , on the total mission time. The method of mission analysis presented in Reference 10 was applied to the round-trip mission to Mars with a 9000 Kg drop-off mass at Mars and a useful payload of 115 Kg returned to Earth. The analysis leading to the desired results is described in the following paragraphs.

The total kinetic power in the exhaust of an ideal rocket engine is determined by

$$P_j = - \frac{1}{2} \frac{dM}{dt} V_j^2 \qquad (2)$$

The magnitude of the thrust acceleration of the vehicle is given by

$$a = - \frac{dM}{dt} V_j /M \qquad (3)$$

The exhaust velocity can be eliminated between equations (2) and (3) and the result integrated to obtain

$$\frac{1}{M} = \frac{1}{M_o} + \frac{J}{2P_j} \qquad (4)$$

where

$$J = \int_{0}^{t} a^{2}\, dt$$

This expression determines the final mass, after each portion of the mission, given the initial mass, the jet power and the value of the integral of the thrust acceleration.

Since the payload and drop-off mass have been specified for the mission, it is most convenient to apply equations (4) to each portion of the mission and solve for the required initial mass as shown in Appendix C.

$$M_{o} = \frac{\dfrac{M_{s} + M_{PL}}{1 - \dfrac{J_{in}}{2P_{j}}(M_{s} + M_{PL})} + M_{Do}}{1 - \dfrac{J_{out}}{2P_{j}}\left[\dfrac{M_{s} + M_{PL}}{1 - \dfrac{J_{in}}{2P_{j}}(M_{s} + M_{PL})} + M_{Do}\right]} \qquad (5)$$

Assuming all of the electrical power generated is used for propulsion, the power in the jet is related to the power generated by the thruster efficiency,

$$P_{jet} = \eta P \qquad (6)$$

The weight of the spacecraft is determined by the power generated and the spacecraft specific mass,

$$M_s = \propto P \qquad (7)$$

Values of J for optimum trajectories to Mars as a function of heliocentric trip time and the wait time at Mars have been calculated in Reference 10. Thus, for specified values of the electrical power level, powerplant specific mass, thruster efficiency, mission time and wait time at Mars the initial mass required for the mission is determined by equation (5).

The analysis in Reference 10 leading to the required values of the integral J is based on the simplifying assumption that the orbits of Earth and Mars are circular and coplanar. Also, an optimum variablethrhust program is used to simplify the calculations for the heliocentric phases of the mission. The jet power is held constant in the optimum thrust program and the thrust and exhaust velocity are allowed to vary to obtain an optimum performance profile. The performance obtained under these assumptions is optimistic compared with that of a realistic nearly constant thrust device. The results obtained, therefore, are treated as an upper boundary or vehicle performance which is sufficiently realistic to show the effects of the various propulsion parameters.

Typical values of $\eta = 0.5$, 0.7 and 0.9 , $\propto_s = 2$, 6 and 10 kg/kwe, and generated power levels of 500,1000, 1500 kwe were used to calculate the required initial mass for a

given total trip time and a wait time at Mars of 48 days. The initial mass values were obtained from a computer program using equation (5). The wait time of 48 days includes two 20 day periods to perform the spiral into and out of a low Mars orbit, and eight days in Mars orbit to pick up the soil samples and return them to the vehicle. Total trip time is the sum of the heliocentric trip time for an optimum trajectory, the time required to spiral into a low earth orbit optimized for the heliocentric trip time, and the 48 day wait period at Mars. The spirals at Mars were not optimized for this mission analysis. The thrust acceleration required for these spirals is small, and small variations from the near optimum 20 day spiral period would have little effect on the desired results.

The results of these calculations are plotted in Figures 1, 2, and 3, for the case of the spacecraft boosted to Earth escape velocity. These figures show the total mission time as a function of the initial mass required for parametric values of α_s, η and generated power level. Total mission time is an indication of powerplant performance for a mission with fixed payloads. The required initial mass is limited to about 45,000 kg, since the vehicle will probably be chemically boosted to Earth escape speed using a Saturn V rocket. Initial mass is thus a constraint on the mission. The curves in Figures

1, 2, and 3 show that the required initial mass increases slowly with decreasing total mission time until the maximum capability of the powerplant is reached. Further reductions in total mission time cause a rapid increase in the mass of the propellant required. This, in turn, causes the initial mass to tend toward infinity.

It is of interest to note in Figure 1 that even for the least favorable values of α_s, η and generated power level, with an initial mass of 45,000 kg, the predicted total mission time is less than 650 days, and well below the maximum time of two years. Comparing the effects of the powerplant parameters for the given initial mass of 45,000 Kg, it can be be seen from Figure 2 for $\eta = 0.07$ and $\alpha_s = 6$ kg/kwe that the difference in total mission time for generated power levels of 500 kwe to 1500 kwe is only about 20 days. The total mission time for a generated power level of 1000 kew, $\alpha_s =$ 6 kg/kwe and for various η from Figures 1, 2, and 3 is: $\eta = .5$, TT - 490 days; $\eta = .7$, TT = 446 days; and for $\eta = .9$, TT = 410 days. The difference in total mission time between $\eta = .5$ to $\eta = .9$ is 80 days. From Figure 2, for $\eta = .7$ and a generated power level of 1000 kwe, the total mission time for various α_s is: α_s - 2 kg/kwe, TT = 321 days, $\alpha_s = 6$ kg/kwe, TT - 446 days; and for α_s = 10 kg/kwe, TT = 525 days. The difference in total mission

EARTH MARS ROUND TRIP MISSION

Total Trip Time vs Initial Mass

(Commencing with Earth escape velocity, terminating in low Earth orbit
with Mars wait time 48 days, drop off mass 9000 kg and payload mass 115 kg)

Total Trip Time vs Initial Mass for Nuclear Electric Propulsion

Spacecraft Specific Mass, $\alpha_S = 2,\ 6,\ 10$ kg/kwe

Optimum variable thrust profile

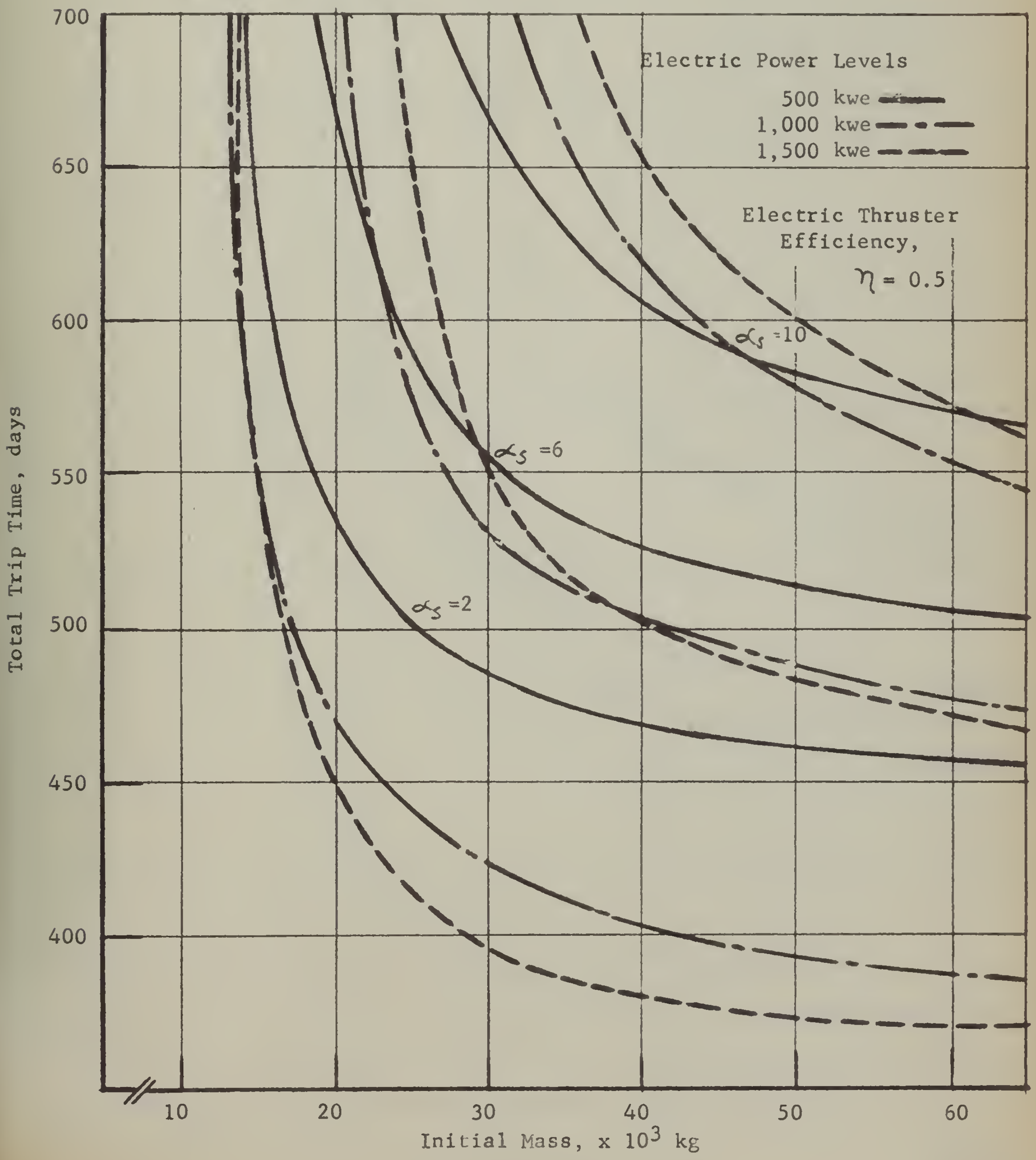

FIGURE 1

EARTH MARS ROUND TRIP MISSION

Total Trip Time vs Initial Mass

(Commencing with Earth escape velocity, terminating in low Earth orbit with Mars wait time 48 days, drop off mass 9000 kg and payload mass 115 kg)

Total Trip Time vs Initial Mass for Nuclear Electric Propulsion

Spacecraft Specific Mass, $\alpha_S = 2, 6, 10$ kg/kwe

Optimum variable thrust profile

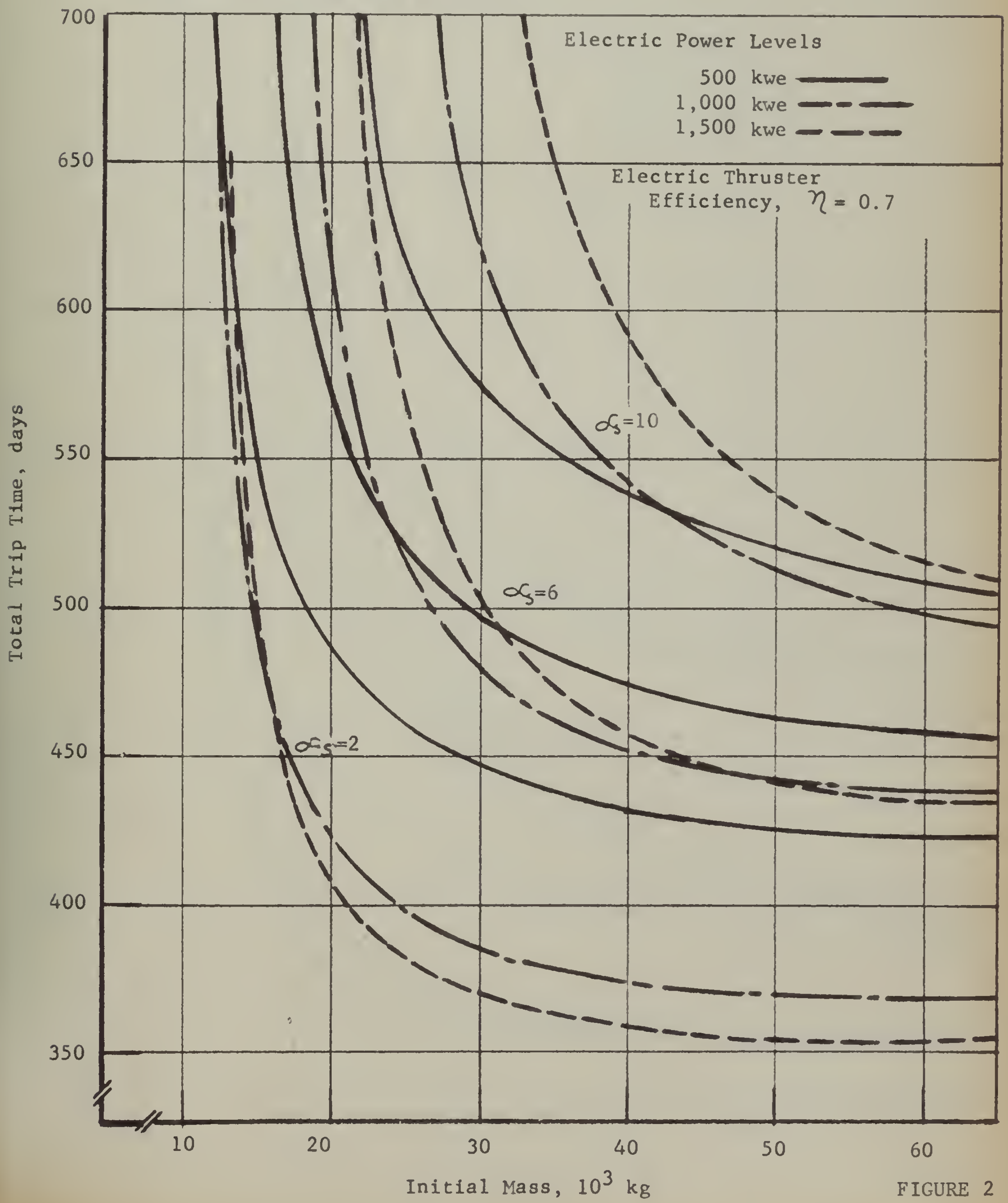

FIGURE 2

EARTH MARS ROUND TRIP MISSION

Total Trip Time vs Initial Mass

(Commencing with Earth escape velocity, terminating in low Earth orbit with Mars wait time 48 days, drop off mass 9000 kg and payload mass 115 kg)

Total Trip Time vs Initial Mass for Nuclear Electric Propulsion

Spacecraft Specific Mass, α_s= 2, 6, 10 kg/kwe

Optimum variable thrust profile

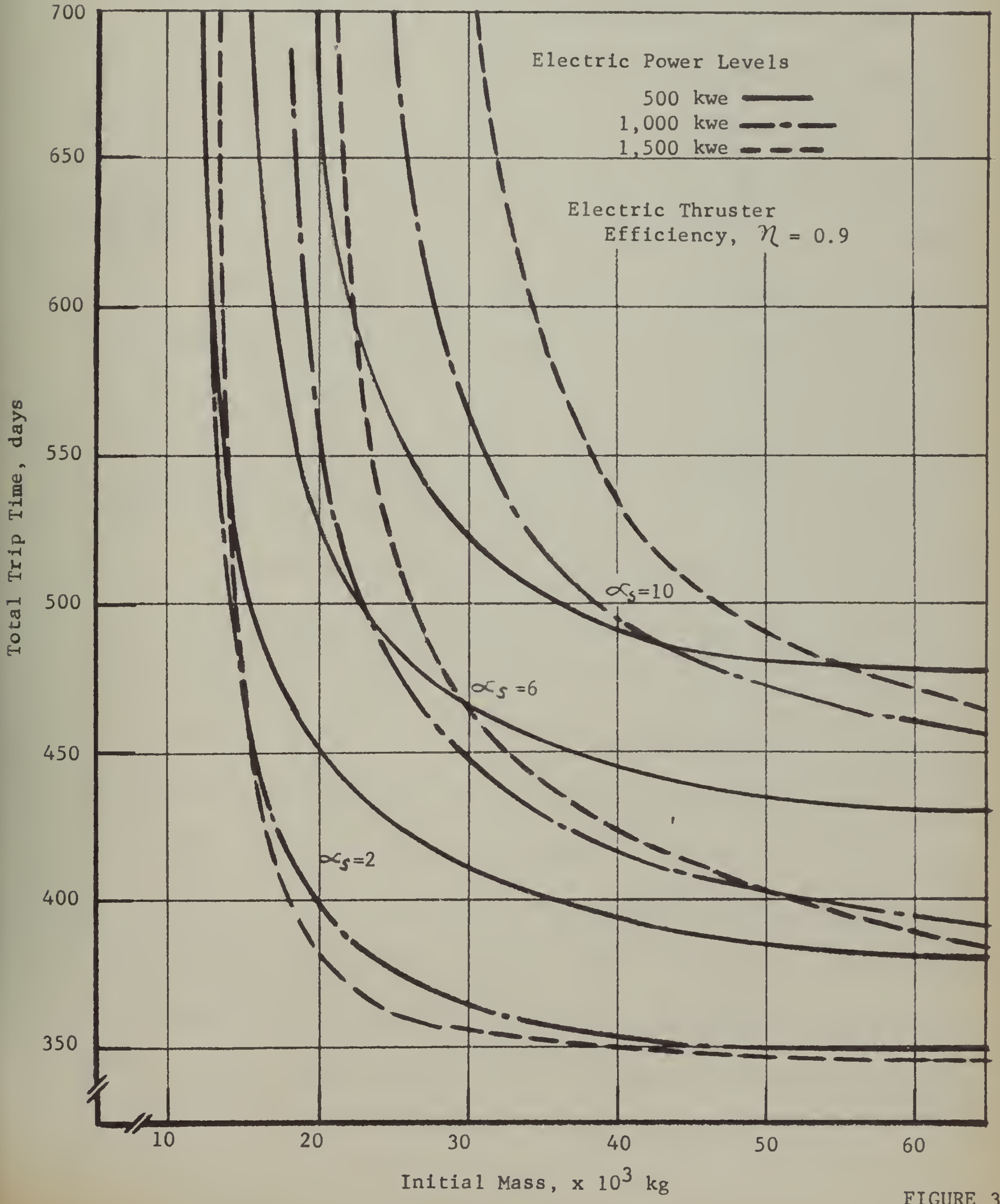

FIGURE 3

time between $\alpha_s = 2$ kg/kwe to $\alpha_s = 10$ kg/kwe is 204 days.

In general the results indicate the large dependence of vehicle performance on the spacecraft specific mass. Also, for the range of power levels considered, the performance is seen to be relatively independent of the power level. It should be noted, however, that this is not entirely true since in most cases α_s will be a decreasing function of power level. The thruster efficiency has a significant effect on performance. Although the results are for fixed values of payload, drop-off mass, and for selected values of powerplant parameters, they indicate the generally accepted fact that the specific mass is the most significant performance parameter.

A similar analysis was made for a mission where the vehicle is spiraled out from low earth orbit instead of boosted to Earth escape speed. The results are shown in Figure 4. For given values of $\eta = .7$, $\alpha_s = 6$ kg/kwe and generated power level of 1000 kwe the total mission time for an initial mass of 65,000 kg is about 500 days. This value can be compared with the total mission time of 446 days for an initial mass of 45,000 kg, with similar values of α_s, η and generated power level, that is boosted to Earth escape velocity. It is evident that whenever it is possible to boost the vehicle

EARTH MARS ROUND TRIP MISSION

Total Trip Time vs Initial Mass

(Commencing and Terminating in Low Earth orbit with
Mars wait time 48 days, drop off mass 9000 kg and payload mass 115 kg)

Total Trip Time vs Initial Mass for Nuclear Electric Propulsion

Spacecraft Specific Mass, α_S= 2, 6, 10 kg/kwe

Optimum variable thrust profile Thruster Efficiency, η = 0.7

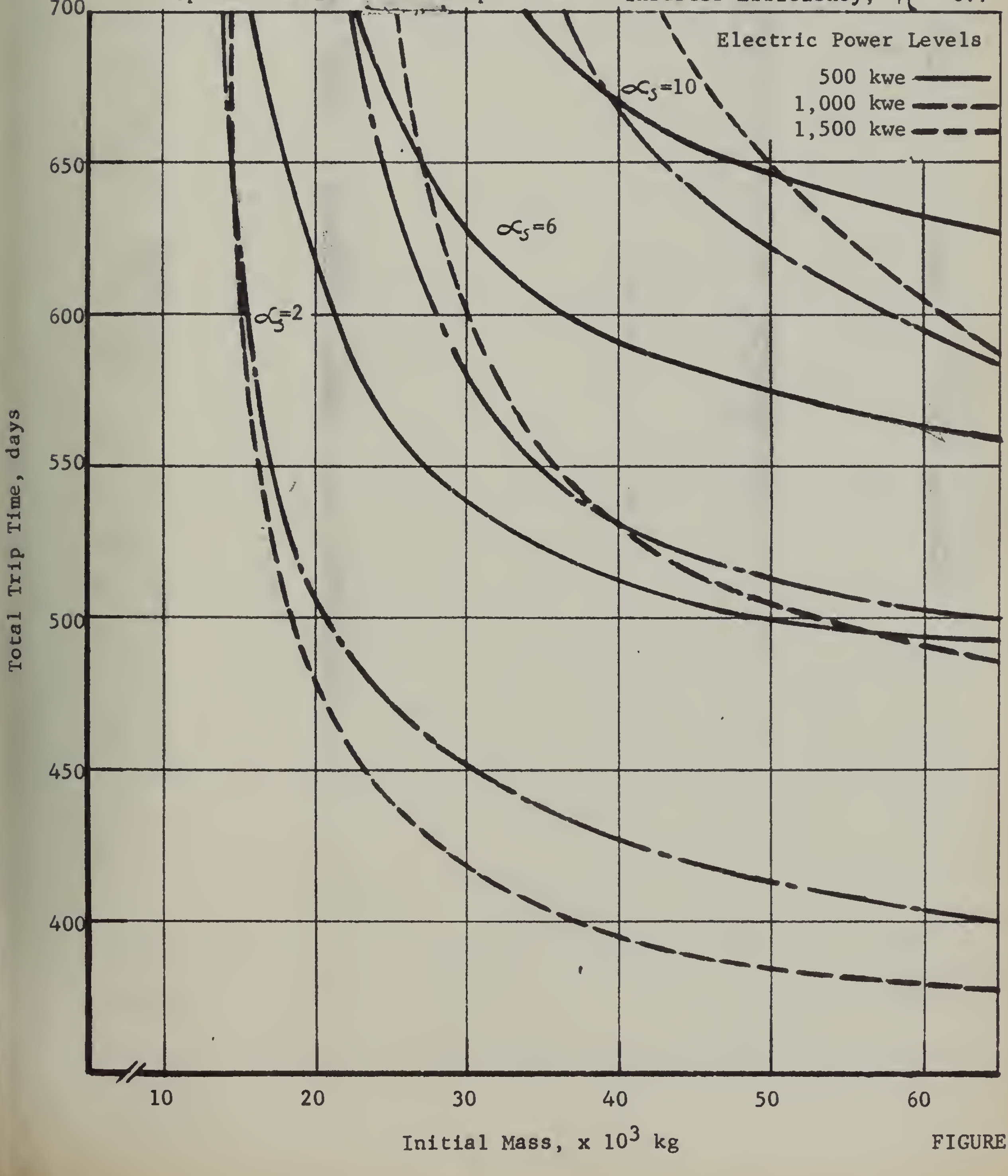

FIGURE 4

to Earth escape velocity, a considerable savings in total trip time will result.

D. Launch Dates and Mission Time

For a long period of time it was believed that all round trips to Mars would be dependent on the cycling of the Mars/Earth relationship in their respective swings around the Sun. The times that Earth and Mars are closest to each other is called the opposition of Mars. Because of the eccentricity of the Martian orbit, the distance varies from approximately 55 million kilometers during a favorable opposition to as much as 103 million kilometers during an unfavorable opposition. The time between successive oppositions, approximately every 25 months, is called the synodic period while the time for a particular opposition to repeat itself is called a synodic cycle. This occurs at 15 and 17 year intervals. (Reference 2).

Two types of round-trip missions to Mars are of importance, opposition class trips and conjunction class trips. An opposition class trip is one in which the vehicle arrives at and departs from Mars over a period of a few days or a few weeks. The conjunction class trip is one in which the vehicle arrives at Mars shortly after one opposition and departs just prior to the following opposition. The opposition class trips are characterized by high energy requirements and high entry

speeds upon returning to Earth; whereas, conjunction class trips generally take longer but require less mass in Earth orbit.

Of the two types of round trips just considered, the opposition class trip appears the most suitable for the selected unmanned round trip mission to Mars, because of the shorter duration required. Unfortunately, for the time period of interest in this analysis, 1975-1985, the oppositions are generally unfavorable until near the end of the period.

This situation is now considerably eased, however, by the discovery of a method to fly opposition trips to Mars utilizing a Venus swingby. By utilizing the gravitational field of Venus in the transfer trajectories, the short duration of opposition class trips can be approached with the low energy requirements of conjunction class trips.

The possibilities of utilizing a Venus swingby for either acceleration or deceleration are numerous. From Reference 11, it is indicated that the velocity requirements of the possible missions through a cycle of favorable to unfavorable opportunities remain approximately the same when utilizing a Venus swingby. This indicates, then, that of all the launch windows within the period of interest, from 1975 to 1985, none possesses a significant advantage over the others. Accordingly,

all of the launch windows during the time period of interest are considered as possible launch dates for the selected unmanned round-trip missions to Mars.

III. POWER SYSTEM ANALYSES

a. Reference Space Nuclear Power System--Rankine Cycle

1. Cycle Description

A schematic of the reference powerplant cycle is depicted in Figure 5. The powerplant uses a Rankine turboelectric cycle with a nuclear reactor energy source and alkali metal working fluids. A two loop indirect cycle was chosen for several reasons. Using a separate reactor coolant loop eliminates the requirement that the reactor serve as a boiler. This frees the reactor design from the problems of a two phase working fluid and allows a minimum volume design and thus minimum shield mass. A separate reactor coolant loop also provides minimum system exposure to an activated working fluid. A three loop cycle is often proposed with the additional heat rejection loop split into several separate segments to reduce system vulnerability to meteroid damage. The use of a third loop was rejected on the basis of the additional mass required for the condensor, pumps and larger radiator operating at a lower temperature. It was felt system reliability could still be maintained using shut off valves to isolate damaged sections of the radiator.

Liquid lithium was chosen as the reactor coolant because of its low vapor pressure at the operating temperature,

LIQUID METAL RANKINE CYCLE NUCLEAR SPACE POWER SYSTEM

Powerplant Schematic

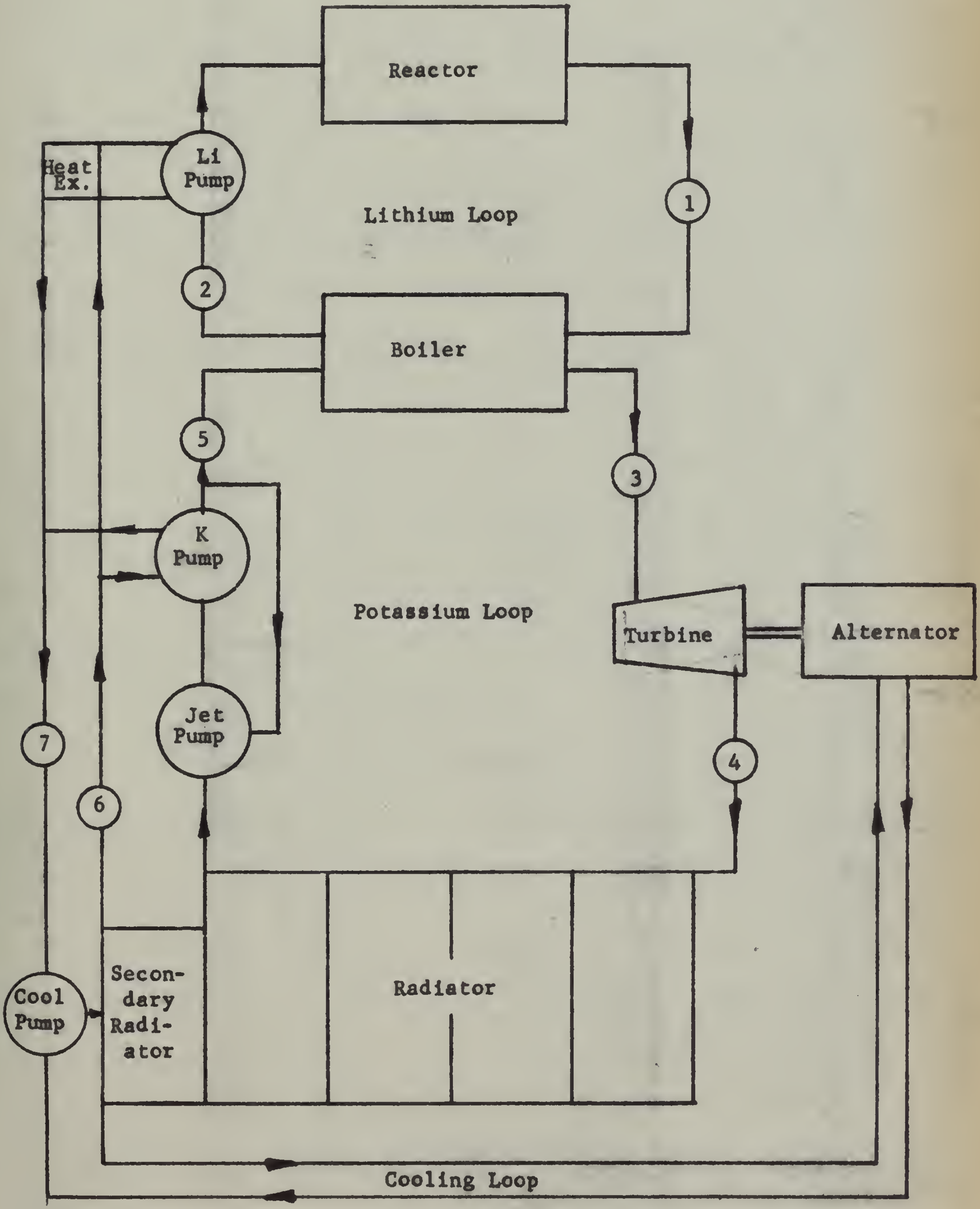

FIGURE 5

its excellent heat conduction properties, its short half-life, and the fact that it absorbs very little radiation. Potassium was selected as the power conversion working fluid because of its good heat conduction properties and proper vapor pressure range at operating temperatures.

A turbine inlet temperature of 1284°K was selected as the maximum operating temperature for the turbine and reactor materials which must be highly corrosion resistant. The radiator temperature of 964°K is then determined by the well known carnot-cycle criterion that the optimum sink is three-fourths of the source temperature since the reference cycle is very nearly a carnot-cycle. The pressures in the cycle are dictated by the fluid vapor pressure. A summary of the pertinent operating conditions and data on the reference liquid metal cycles is contained in Table I.

Physically, the powerplant consists of the reactor, conical shadow shield, boiler, turbine, generator, radiator and the necessary pumps to circulate the fluids. The reactor coolant is piped to the boiler which is located in a containment vessel along with the turbine, generator, pumps and other power conversion equipment. The potassium working fluid is heated in the boiler and then passed through the turbine out to the surrounding conical radiator and back to the pump. The

TABLE I

Liquid Metal Rankine Cycle

Cycle Characteristics and Data

Cycle Temperature, Pressure and Vapor Quality

Station	1	2	3	4	5	6	7
Temperature (°K)	1367	1311	1284	964	881	575	616
Pressure (kg/cm^2)	1.28	0.70	6.67	0.50	7.38	4.50	1.00
Vapor Quality (%)	Liq.	Liq.	100	85.5	Liq.	Liq.	Liq.

Cycle Data

Generator Output Power Level (kw)	500	1000	1500
Lithium Flow Rate (kg/sec)	12.95	25.84	38.80
Potassium Flow Rate (kg/sec)	1.345	2.690	4.045
Reactor Power Density (kwt/kg)	7.5	10.3	12.0
Reactor Thermal Power (kwt)	2940	5870	8310
Boiler Power (kcal/sec)	700	1399	2100
Primary Radiator Condensing Power (kcal/sec)	551.0	1103.0	1657.4
Primary Radiator Sub-cooler Power (kcal/sec)	21.6	43.0	64.6
Primary Radiator Total Power (kcal/sec)	572.6	1146.0	1722.0
Primary Radiator Area (m^2)	64.5	128.8	193.4
Secondary Radiator Power (kcal/sec)	36.8	73.2	118.7
Secondary Radiator Area (m^2)	2.7	5.4	8.7
Total Radiator Area (m^2)	67.2	134.2	202.1
Lithium Pump Power (kw)	8.00	15.50	21.75
Potassium Pump Power (kw)	2.50	5.50	7.50
Potassium Coolant Pump Power (kw)	0.75	1.50	2.50

final portion of the primary radiator is a sub-cooler where the temperature of the fluid is lowered to prevent cavitation in the potassium pump. The pumps and generator are cooled and lubricated by an auxiliary potassium circuit which dumps its heat into the secondary radiator. A description of the cycle components and the methods used to size and determine their mass is given in the following paragraphs.

2. Component Masses

a. Reactor

The most commonly proposed heat source for the Rankine cycle system is an alkali-metal cooled nuclear reactor. The technology for this type of reactor has evolved from various military and conventional applications and is considered fairly adaptable to space application. The reactor operates at a high fluid outlet temperature equal to 1367°K (2000°F). The use of lithium as a reactor coolant requires the use of corrosion resistant columbium alloys throughout the liquid loop.

Compactness is generally achieved through the use of a fast-neutron reactor utilizing such core materials as metallic carbides fueled with dispersed uranium carbide, Reference 12. The carbides can be protected from the liquid lithium by a material such as columbian 1 per cent zirconium alloy,

C_b - 1Zr. The primary disadvantages of a fast nuclear reactor are the increased shielding problems and high fuel inventory which tends to degrade the mechanical integrity of the fuel matrix material at high temperatures.

For the reference Rankine cycle, no attempt has been made to describe the reactor in more detail other than the considerations already presented. Therefore, in order to determine the reactor masses required for the three reference cycles, a graph of reactor power density versus reactor power was constructed in Figure 6 from the data available in the unclassified literature. The two points most heavily weighed were those for the 35 kwe SNAP 8 reactor, Reference 13, and the 1.2 mwe GE design, Reference 14. The resultant power densities for the cycles considered are indicated on Figure 6 and the corresponding masses are listed in Table II.

b. Turbine and Generator

The basis for the turbine design was taken from the 300 KVA turbogenerator presented in Reference 14. The subject turbines were then sized by scaling the last stage mean rotor diameter directly with the square root of power, from Reference 17, i.e.,

$$D \propto (P)^{1/2} \qquad (8)$$

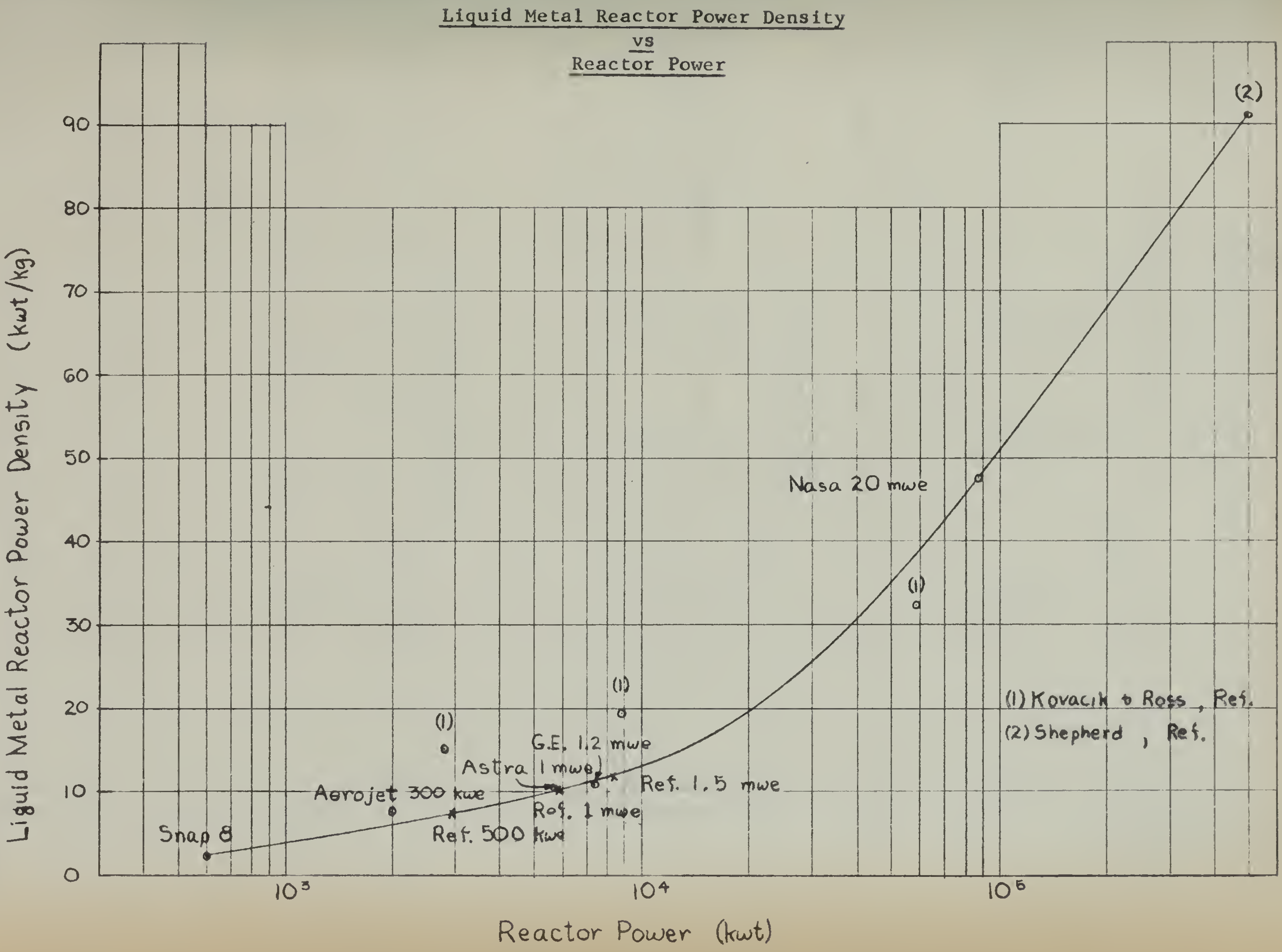

Liquid Metal Reactor Power Density
vs
Reactor Power

FIGURE 6

TABLE II

Liquid Metal Rankine Cycle

Reactor Masses

System	Output		Mass (kg)	Power Density (kwt/kg)
	kwe	kwt		
SNAP 8	35	600	273	2.2
Aerojet	300	2,000*	260	7.7
NASA (English)	20,000	88,000	1,850	47.5
General Electric	1,200	7,400	683	10.85
Astra	1,000	5,730	545	10.5

*Overall efficiency estimated at 15%.

Turbogenerator Mass

Power Level (KVA)	300*	500	1,000	1,500
Mean Diameter (cm)	21.3	27.6	39.1	48.0
Turbine Mass (kg)	120.5	202.2	388.5	609.0
Generator Mass (kg)	159.5	253.0	442.0	620.0
Total Mass (kg)	280.0	455.2	830.5	1229.0

*Basic G.E. design Ref.

Liquid Metal Pump Masses

Pump Power (kwe)	Type Pump	Mass (lb)*	Mass (kg)
60	Li	360	163.5
16	K	150	68.2
5.3	NaK	110	50.0
2.5	NaK	60	27.3

*Basic G.E. design Ref.

The masses of the desired turbines were obtained by considering the mass to vary directly with rotor area. The resultant masses are presented in Table II.

The masses of the subject generators, Mg, were obtained directly from the relation:

$$M_g = \frac{(1.304)\ (P)}{(P)^{0.157}} \qquad (9)$$

This expression was developed with the use of actual aircraft generator masses in Reference 18. The results are listed in Table II.

The total masses of the combined turbogenerator have been plotted versus generator capacity in Figure 7. The designs presented in Reference 14 in addition to the basic 300 KVA design have been indicated on Figure 7 to show the good agreement with the curve of scaled values. All generators discussed here are assumed to be of the 600/1000 volt class operating at approximately 2000 cps.

c. Radiator

The removal of waste heat in the Rankine cycle is accomplished by means of two space radiators. The first part of the primary radiator is a direct condensing radiator where the working fluid is condensed from the vapor

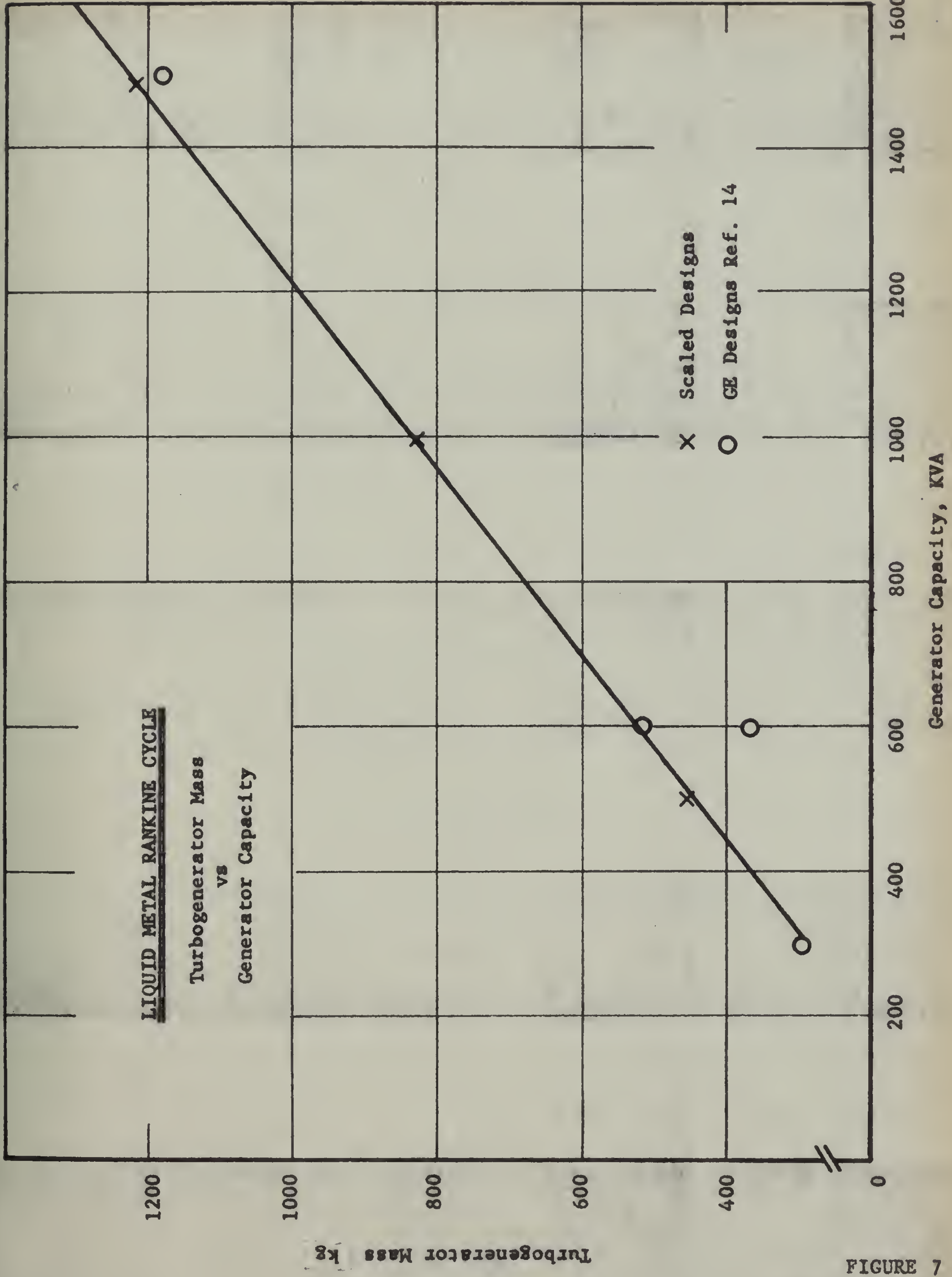

LIQUID METAL RANKINE CYCLE

Turbogenerator Mass
vs
Generator Capacity

FIGURE 7

state into the liquid state. This part of the primary radiator operates at a constant temperature, rejecting the heat of vaporization into space. The second part of the primary radiator and the secondary radiator actually cools the liquid and thus lowers the temperature of the working fluid.

The required radiator area for both liquid metal and gas turboelectric cycles has been treated previously by many authors and hence will not be derived here. The actual formulas used, however, and their underlying assumptions are presented.

For the condensing portion of the primary radiator, from Reference 19,

$$A_R = \frac{1}{\sigma f \ T_4^4 \ \epsilon} \ Q \qquad (10)$$

where it is assumed that radiator surface temperature is equal to the fluid temperature in the radiator. For this analysis, values of $\epsilon = .90$ and $f = .85$ were used. The required radiator areas for the subcooler of the primary radiator and the secondary radiator were determined from the following formula also obtained from Reference 19:

$$A_R = \frac{w c_p}{3 \sigma \epsilon f \ (T_5)^3} \left[1 - \left(\frac{T_5}{T_4} \right)^3 \right] \qquad (11)$$

where it is assumed that fluid heat loss is equal to the radiated heat loss. In both equations the small effect due to a finite sink temperature is neglected. The required radiator areas for the three power levels are listed in Table I along with the necessary heat loads and flow rates required for the calculations.

Many concepts and schemes have been proposed for the construction of space radiators. The design that has received the most support for the liquid metal Rankine cycle is the cylindrical and/or conical shaped tube and fin type radiator. Its primary advantage is that it is easily stressed for launch and can be conveniently packaged in presently conceived boosters.

Two of the more recent designs of this type are presented in Reference 14 and Reference 20. One is fabricated primarily of Beryllium, the other of stainless steel and copper. Both are designed for a meteroid penetration probability of 0.95. Adding together the individual masses of each design, including the tubes, fins, headers and associated structure, the specific radiator mass varies from 14.65 kg/m^2 for a 300 kwe system to 12.20 kg/m^2 for a 1,200 kwe system. The specific masses of the radiators for the liquid metal Rankine cycle were determined by scaling the specific mass between the above limits with power level. The resultant radiator masses are presented in Table III.

TABLE III

Liquid Metal Rankine Cycle

Powerplant Mass Breakdown

Generator Output Power Level (kw)	500	1000	1500
Reactor and Primary System			
Reactor	392	570	692
Lithium Pipe (wet)	14	26	34
Lithium Pump (with heat exchanger)	53	69	82
Reactor and Primary System Mass (kg)	459	665	808
Power Conversion System			
Boiler	140	240	340
Potassium Pump	30	43	51
Potassium Jet Pump	7	11	15
Potassium Coolant Pump	13	22	30
Potassium Piping	69	138	207
Pressurizer, Accumulator and Valves	47	93	140
Turbine and Generator	446	833	1225
Controls	68	68	68
Pump Power Supply	2	4	6
Containment Tank	64	118	166
Power Conversion System Mass (kg)	886	1570	2248
Radiator			
Primary	945	1342	1830
Secondary	40	79	128
Fluid Inventory	112	290	437
Radiator Mass (kg)	1097	1711	2395

Total Powerplant Mass (kg)	2442	3946	5451
Powerplant Specific Mass (kg/kwe)	4.89	3.95	3.64

The liquid potassium inventory was determined for the condensing radiator on the basis that the liquid volume was equal to sixty percent of the void area. The potassium specific mass for the non-condensing radiators was estimated at 2.16 kg/m^2 of radiating area.

d. Boiler

The potassium boiler is a tube and shell configuration. The potassium is vaporized in the tubes that are heated by the liquid lithium flowing in the shell. It operates at a potassium inlet pressure of 7.38 kg/cm^2 and temperature of 881°K and is fabricated from Cb-1Zr alloy. The mass of the boiler was estimated using the boiler designs contained in Reference 21. These designs were based on a computer program used to calculate the length of tube required to vaporize the potassium to 100 percent quality dependent on the inlet conditions. The boiler mass was then plotted in Reference 21 as a function of the number of tubes using the outside tube diameter as a parameter. The boilers for the reference liquid metal cycle were scaled from these plots based on a constant mass flow rate per unit area.

e. Pumps, Piping and Associated Equipment

Three motor driven centrifugal pumps are

required in the reference liquid metal cycle to circulate the fluids. They are: a lithium pump for the reactor coolant, a potassium pump for the working fluid and a potassium pump for the coolant used to cool the generator and the pumps themselves. The two potassium pumps are cooled and lubricated by circulating potassium coolant through the pump. The lithium pump is cooled and lubricated by lithium which dumps heat to the potassium coolant loop through a heat exchanger. The pumps were sized on the basis of the required pumping power using the formula,

$$\text{Pumping Power} = \frac{\Delta p\, AV}{\eta_p} = \frac{\Delta p\, w}{\eta_p \rho} \qquad (12)$$

Overall pump efficiency was taken to be $\eta_p = 0.57$. The pressure drops through the components and piping were taken from design information or estimated to obtain the pumping power. Pump mass is plotted as a function of pump power in Figure 8. The curve was obtained using similar pump designs from Reference 14. The mass of each pump in the reference liquid metal cycle was then obtained from Figure 8 based on the calculated power required. The pump electrical requirements are supplied by a pump power supply consisting of a frequency converter from 2000 cps to 167 cps.

A jet pump is used in the potassium loop to

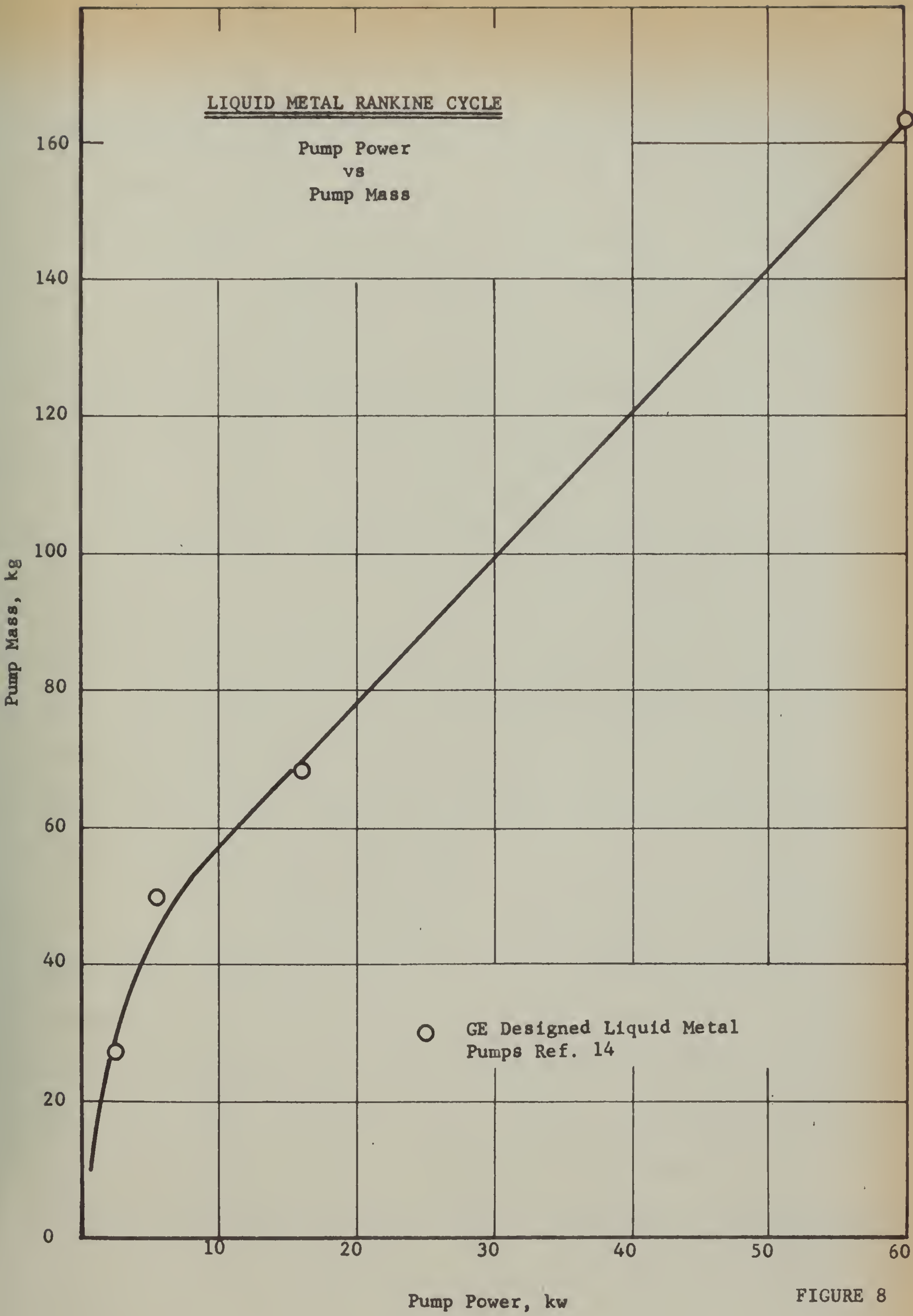
LIQUID METAL RANKINE CYCLE
Pump Power
vs
Pump Mass
Pump Mass, kg
0
20
40
60
80
100
120
140
160
10
20
30
40
50
60
Pump Power, kw
GE Designed Liquid Metal
Pumps Ref. 14

FIGURE 8

obtain sufficient pressure to prevent the centrifugal potassium pump from cavitating. The mass of the jet pump was estimated at half the mass of the potassium coolant pump.

All of the piping is fabricated from C_b-1Zr alloy. The size and mass of the pipes connecting the reactor and boiler in the lithium loop were calculated using a flow velocity of 6m/sec. The pipes have meteroid armor sufficient to provide a non-puncture probability of 95 percent for 10,000 hours of operation. The mass of the piping and valves for the potassium loop inside the power conversion container was scaled from the design data in Reference 14 on the basis of mass flow rate. An accumulator is provided in the potassium loop and a pressurizer in the lithium loop to provide for fluctuation in fluid level. Their masses were scaled from the data in Reference 14 based on mass flow rate.

The cylindrical vessel enclosing the power conversion equipment is formed by two circular bulkheads separated by a structural support and enclosed with a light honeycomb construction. The turbogenerator is mounted on the structural support and the boiler, pumps and associated equipment are mounted on the end bulkheads. The mass of this structure was scaled from the data in Reference 14 proportional to the mass of the components inside the containment vessel.

The mass of the powerplant controls was taken as 68 kg again based on the data in Reference 14.

A complete mass breakdown of all the components in the liquid metal Rankine cycle is presented in Table III. The resultant powerplant specific masses for the reference cycle were found to be 4.89 kg/kwe at 500 kwe, 3.95 kg/kwe at 1000 kwe and 3.64 kg/kwe at 1500 kwe.

B. Brayton Cycle Space Nuclear Power System

1. Cycle Description

A schematic of the Brayton turboelectric powerplant cycle is depicted in Figure 9. The powerplant uses a nuclear reactor energy source and an inert gas working fluid. Power conversion is accomplished in the turboelectric cycle and the waste heat is rejected by means of a space radiator. As in the Rankine cycle, several Brayton cycle configurations have been proposed which employ from one to three loops. A single loop cycle was selected for minimum system complexity.

It was felt that a separate reactor cooling loop was not required in the Brayton cycle. The major reactor design problem of two phase flow which dictates a separate reactor coolant loop in the Rankine cycle is no longer a problem in the single gas phase Brayton cycle. Activation of the inert gas

BRAYTON CYCLE NUCLEAR TURBOELECTRIC

Powerplant Schematic

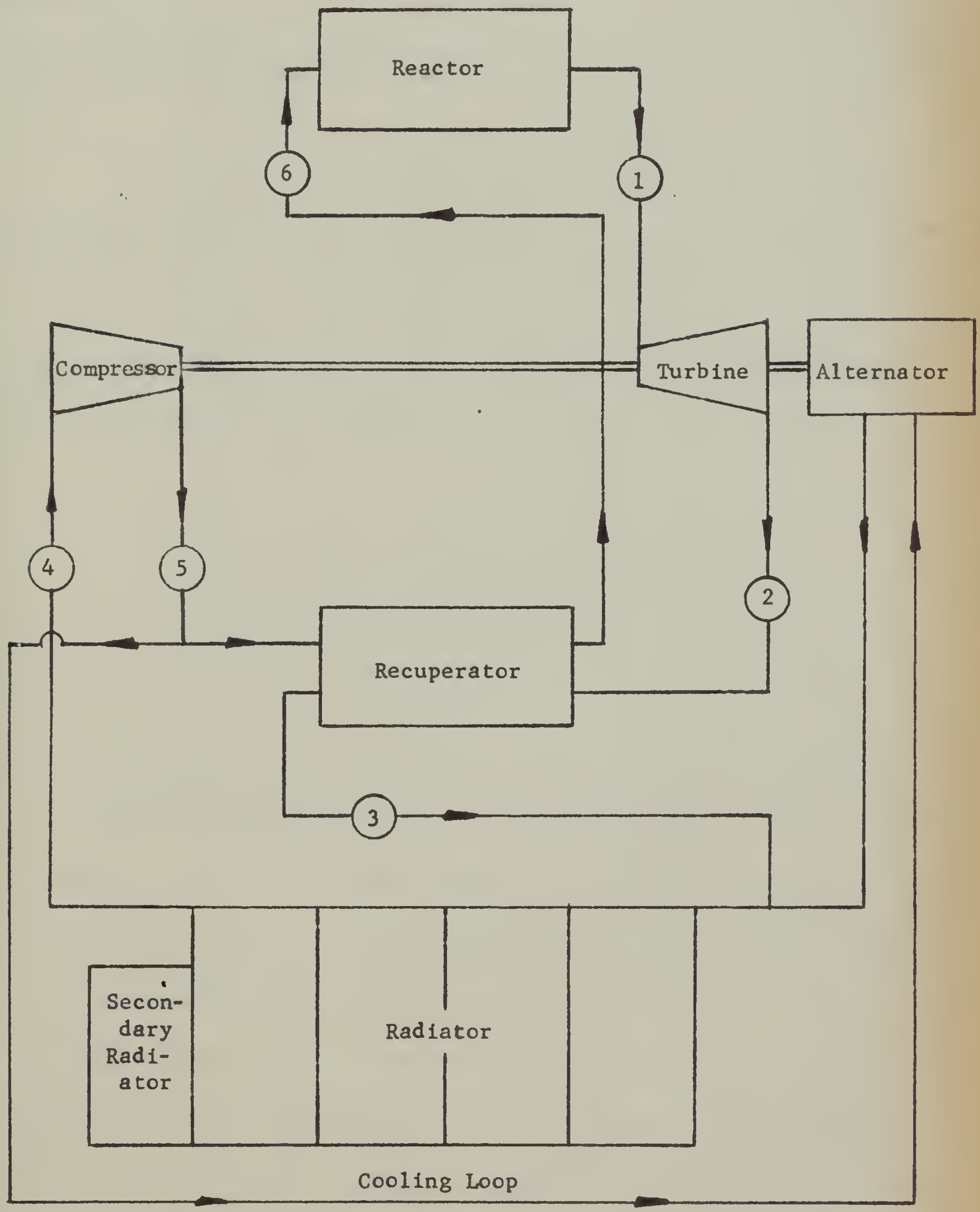

FIGURE 9

fluid in the reactor and subsequent irradiation of the payload in the single loop cycle is not considered a problem. The radiation dose to the payload from an inert gas working fluid is negligible for any unmanned applications as stated in Reference 22.

The use of a third loop to accomplish the heat rejection for the cycle is considered undesirable because of the additional mass required in the heat exchangers and larger radiator. As in the liquid metal cycle, it is believed that system reliability can be maintained without the use of a third loop.

2. Thermodynamic Characteristics of the Brayton Cycle

Brayton cycle performance is a function of many parameters. The primary variables are the choice of the working fluid, maximum cycle temperature and pressure, component pressure losses, generator and turbine efficiency, recuperation effectiveness, turbine temperature ratio and the compressor inlet to turbine inlet or cycle temperature ratio. The working fluid and maximum cycle temperature and pressure should be selected with due regard for material limitations and their effects on the other parameters of the system. The rest of the parameters can then be used to optimize the cycle to obtain a minimum mass, highly efficient system. Cycle efficiency is

is of importance only in so far as it affects the mass of the system, since the energy source is a nuclear reactor and, therefore, the energy supply is not limiting to the sytem.

a. Working Fluid

The inert gases are viewed as the best choice for a working fluid because of their lack of chemical interaction with structural and containment materials at high temperatures. The choice of the particular inert gas to be used centers around its effect on the heat transfer and turbomachinery components of the cycle. A low molecular weight fluid such as helium has a relatively high heat transfer coefficient but requires a large number of compressor and turbine stages which tends to increase the complexity and degrade the efficiency of the turbomachinery components. A high molecular weight fluid such as xenon has very poor heat transport properties but requires the minimum number of turbomachinery stages. There is thus an apparent compromise in the selection of a working fluid suggesting a medium molecular weight inert gas such as neon or argon.

Fortunately, there is even a better solution. As shown in Reference 23, the transport properties of a mixture of inert gases are not a linear function of the volume fraction of each gas. Indeed, the heat transfer characteristics of an

inert gas mixture are frequently better than for either of the gases considered separately, particularly in the case of a helium and xenon gas misture. Also, with gas mixtures, the molecular weight of the gas is a running variable for the designer to select to best advantage instead of selecting discreet values dictated by the choice of a particular compromise fluid such as neon or argon.

In view of the above discussion, a mixture of helium and xenon gases with a molecular weight of thirty was chosen as the working fluid for the Brayton cycle powerplant. The molecular weight of thirty was selected since it gives the highest heat transfer coefficient for an inert gas mixture, which is almost one and one-half times the helium heat transfer coefficient, and will result in a reasonable number of stages in the turbomachinery components.

b. Temperature Level

The highest possible maximum cycle temperature is desirable since the corresponding high radiator temperatures produce a minimum of required radiator area. Radiator area is inversely proportional to the radiator temperature to the fourth power. Thus, considerable savings in system mass can be achieved by reducing the size of the radiator which is

the heaviest component in the system. The maximum cycle temperature is dictated by material temperature limitations in the turbine and reactor. From conversations with personnel at the Lawrence Radiation Laboratory, Livermore Site, it is felt that reactor materials present no serious problems for the cycle temperatures of up to 1920°K now being considered. The turbine inlet temperature then becomes the determining factor.

The choice is to go to refractory materials for turbine fabrication or to use cooled blades. Cooling the blades results in a sizeable decrease in turbine efficiency, added turbine complexity and turbine mass. Some thought has been given by the personnel at the Lawrence Radiation Laboratory to a graphite helical turbine which presently has a low forecast efficiency of approximately $\eta_t = 0.80$. Another consideration would be a tungsten alloy turbine using some of the high temperature, high strength alloys such as reported in Reference 24. In addition to material temperature limitations, some thought should be given to the increase in the number of stages and lower operating speeds required at high inlet temperatures as shown in Figure 11 of Reference 22. This figure indicates that a tungsten alloy turbine with argon as a fluid requires eight stages at an operating temperature of 3000°R (1665°K).

In view of the above, it seems reasonable to predict that two maximum turbine inlet temperature levels will be available by the time of this mission; i.e., a 1665°K turbine inlet temperature with a turbine efficiency comparable with present day turbines, and a 1920°K turbine inlet temperature with a considerably reduced turbine efficiency. The former was selected for the Brayton cycle powerplant on the basis that the turbine is less complex, closer to the current turbine technology and because the optimum radiator temperature for a 1920°K turbine inlet temperature exceeds the limits for beryllium, the most promising radiator material. Higher temperature radiator materials such as stainless steel and molybdenum have a radiator mass of about four times that of a beryllium radiator as shown in Reference 22.

c. Pressure Level

Pressure level effects on the Brayton cycle are important primarily in the heat transfer and turbomachinery components. The heat transfer coefficient is proportional to the square of the pressure and turbomachinery size decreases with increasing pressure. Reference 22 states there is a pressure limit dictated by system structural considerations at a compressor outlet pressure of about 500 psia (35.2 kg/cm^2).

Hence, the maximum cycle pressure for the Brayton cycle power plant was set at 35.2 kg/cm^2 to obtain the best heat transfer conditions. The size of the turbomachinery components for the power range of interest, 500 to 1500 kwe, is adequate to insure high component efficiencies at this pressure level.

3. Brayton Cycle Optimization

Having selected the cycle working fluid, a helium and xenon gas mixture with a molecular weight of 30, the cycle maximum temperature, 1665°K, and the cycle maximum pressure, 35.2 kg/cm^2, the next step is to optimize the remaining parameters for a minimum mass system. The Brayton cycle is very sensitive to pressure losses and turbine and compressor efficiencies. A total system pressure loss of $1 - r_t/r_c = 0.1$, where r_t/r_c is the turbine to compressor pressure ratio, was selected as a reasonable value. A compressor efficiency of $\eta_c = 0.85$ and a turbine efficiency of $\eta_t = 0.91$ were taken based on two assumptions: (1) the high temperature tungsten alloy turbine would have an efficiency comparable with today's turbine technology, and (2) the stages of the turbine driving the compressor are at the low temperature end of the turbine and hence can run at the higher speed necessary to obtain today's compressor efficiencies. These efficiencies are comparable with the component efficiencies for a similar 100 kwe Brayton cycle

space powerplant designed in Reference 25 with a turbine inlet temperature of 1960°R (1088°K) and are considered to represent today's technology.

The recuperation effectiveness of E = 0.85 was selected as a reasonable design value as indicated in Reference 22. The effectiveness of the recuperator in the design in Reference 25 is E = 0.86. The two remaining parameters, turbine and cycle temperature ratio, can thus be optimized to obtain a minimum mass system as described in the following paragraphs.

With the masses of the turbine, compressor and reactor considered constant and the assumption that the mass of the recuperator of a given effectiveness varies little with the turbine and cycle temperature ratios, a radiator of minimum mass produces a minimum mass system. And since the mass of the radiator is proportional to the required radiator area, radiator area was chosen as the optimizing parameter. The selection of radiator area as a parameter indicating overall system is consistent with other authors in the field.

An analysis of the Brayton cycle to obtain the required radiator area was performed following the method in Reference 26. The analysis is based on the assumption of an adiabatic system with an ideal gas working fluid. The assump-

tion of a perfect gas for the inert gases is a good one based on the data of Reference 27. Using the notation of Figure 9, the turbine and compressor work are given by the expressions,

$$\Delta h_T = WC_p(T_1 - T_2) \qquad \Delta h_c = WC_p(T_5 - T_4) \tag{13}$$

where $C_p = 0.1657$ kcal/kg °K , $T_1 = 1665$ °K and T_2/T_1 and T_4/T_1 are the optimization parameters.

The required flow rate of working fluid is then given by the ratio of the net shaft power to the net work per pound of fluid by the expression,

$$w = \frac{0.2389\ P}{\eta_g\ C_p\ [(T_1 - T_2) - (T_5 - T_4)]} \tag{14}$$

where the generator efficiency is taken as $\eta_g = 0.95$. The outlet temperature of the compressor, T_5 , is already specified by the compressor and turbine relationship,

$$\frac{T_5}{T_4} = 1 + \frac{1}{\eta_c}\left[\frac{P_5}{P_4}^{\frac{\gamma-1}{\gamma}} - 1\right] \tag{15}$$

with the turbine compression ratio given by:

$$\left(\frac{P_5}{P_4}\right)^{\frac{\gamma-1}{\gamma}} = \left(\frac{1}{r_t/r_c}\right)^{\frac{\gamma-1}{\gamma}}\left(\frac{P_1}{P_2}\right)^{\frac{\gamma-1}{\gamma}} ; \left(\frac{P_1}{P_2}\right)^{\frac{\gamma-1}{\gamma}} = 1 - \frac{1}{\eta_T}\left(1 - \frac{T_2}{T_1}\right) \tag{15A}$$

and $\gamma = 1.667$, $\frac{r_t}{r_c} = 0.9$, $\eta_c = .85$ and $\eta_t = .91$. Thus the required mass flow rate is completely determined by equation 14 for given ratios of T_2/T_1 and T_4/T_1.

The expression for the required specific radiator area which is derived in Reference 26 is given by,

$$\frac{A_R}{p} = \frac{\acute{W}_{cp}}{P} \left\{ \frac{1}{h_R} \ln \frac{T_{w_3}{}^4 - T_{sk}{}^4}{T_{w_4}{}^4 - T_{sk}{}^4} + \frac{1}{4\sigma\epsilon\, T_{sk}{}^3} \left[\ln \frac{(T_{w_3} - T_{sk})(T_{w_4} + T_{sk})}{(T_{w_4} - T_{sk})(T_{w_3} + T_{sk})} \right.\right.$$
$$\left.\left. - 2\left(\arctan \frac{T_{w_3}}{T_{sk}} - \arctan \frac{T_{w_4}}{T_{sk}}\right) \right] \right\} \qquad (16)$$

where the radiator inlet temperature, T_3, is obtained from a relationship for the recuperator of effectiveness, $E = 0.85$,

$$T_3 = T_2 - E(T_2 - T_5) \qquad (17)$$

and the required radiator tube or wall temperatures are given by,

$$T_x = T_{wx} + \frac{\sigma\epsilon}{h_R} (T_{wx}{}^4 - T_{sk}{}^4) \qquad (18)$$

Equation (5) includes the effects of a sink temperature, $T_{sk} = 222^{\circ}K$ and the temperature drop between the gas and the radiator tube wall for a heat transfer coefficient of $h_R = .0678 \ \frac{kcal}{m^2 sec ^{\circ}K}$. The effect of the sink temperature is minor, on the order of one percent at these radiator temperatures. But, the effect of the temperature drop at the tube wall (as much as $100^{\circ}K$ in some cases) on the required radiator area is significant.

The value of the specific radiator area as a function of the turbine and cycle temperature ratios is now completely determined by equations 14, 16, 17 and 18. These equations were set up in the digital computer program contained in Appendix E, which was used to calculate the required specific radiator area for ranges of turbine temperature ratio of $T_2/T_1 = 0.70$ to 0.85 and cycle temperature ratio of $T_4/T_1 = 0.250$ to 0.475. The results of these calculations are recorded in Table IV and presented graphically in the bottom half of Figure 10.

Figure 10 shows that there is a particular value of the cycle temperature ratio which minimizes the required radiator area for each turbine temperature ratio. The optimum cycle is obtained with a turbine temperature ratio, $T_2/T_1 = 0.75$, and a cycle temperature ratio, $T_4/T_1 = 0.35$, which requires a specific radiator area of 0.287 m^2/kwe. The turbine and compressor pressure ratios are then determined by equations (15A) for an optimum value of the turbine temperature ratio. A summary of the pertinent operating conditions and cycle data for the Brayton cycle powerplants is contained in Table V. Compressor pressure ratio and the cycle temperature ratio are frequently used to optimize the Brayton cycle as shown in Reference 19. In effect this analysis uses the turbine temperature ratio in place of the compressor pressure ratio as an optimizing parameter.

TABLE IV

Brayton Cycle

Specific Radiator Area Optimization

T_1 = 1665°K

	Specific Radiator Area, A_R/P m^2/ kwe				
T_4/T_1	T_2/T_1=.70	T_2/T_1=.75	T_2/T_1=.785	T_2/T_1=.80	T_2/T_1=.85
.300	.312	.324	.347	.362	.450
.325	.297	.298	.314	.326	.400
.350	.299	.287	.297	.306	.370
.375	.324	.293	.295	.301	.358
.400	.394	.320	.310	.314	.365

T_1 = 1525°K

.300	.433	.450		.504	.627
.325	.408	.410		.450	.552
.350	.408	.392		.419	.508
.375	.439	.397		.410	.488
.400	.529	.432		.423	.493

T_1 = 1385°K

.300	.627	.652		.732	.913
.325	.585	.589		.648	.797
.350	.580	.559		.599	.726
.375	.620	.562		.580	.692
.400	.740	.605		.595	.695

T_1 = 1245°K

.300	.959	1.000		1.112	1.140
.325	.884	.893		.983	1.121
.350	.868	.839		.900	1.109
.375	.919	.835		.865	1.103
.400	1.109	.893		.879	1.103

TABLE V

Brayton Cycle

Cycle Characteristics and Data

Cycle Temperature and Pressure

Station	1	2	3	3w	4	4w	5	6
Temperature (^{o}K)	1665	1249	938	906	583	578	883	1195
Pressure (kg/cm^2)	33.80	15.10	14.99	-	14.19	-	35.18	35.08

Cycle Data

Generator Output Power Level (kwe)	500	1000	1500
Working Fluid Flow Rate (kg/sec)	6.55	13.09	19.64
Reactor Core Diameter (cm)	34.0	43.0	49.5
Reactor Thermal Power (kw)	2380	4800	7130
Turbine Power (kcal/sec)	451	903	1355
Compressor Power (kcal/sec)	326	651	978
Recuperator Power (kcal/sec)	288	576	865
Recuperator Heat Transfer Area (m^2)	39.1	78.1	117.3
Primary Radiator Area (m^2)	113.8	227.5	341.0
Secondary Radiator Area (m^2)	4.6	9.2	13.8
Total Radiator Area (m^2)	118.4	236.7	354.8
Number of Design Radiator Panels	4.7	9.4	14.0

Cycle Parameters

Turbine Efficiency	0.91
Compressor Efficiency	0.85
Recuperator Effectiveness	0.85
Generator Efficiency	0.95
Compressor Pressure Ratio	2.46
Turbine Pressure Ratio	0.448

BRAYTON CYCLE

Specific Radiator Area

vs

Compressor Inlet to Turbine Inlet
Temperature Ratio

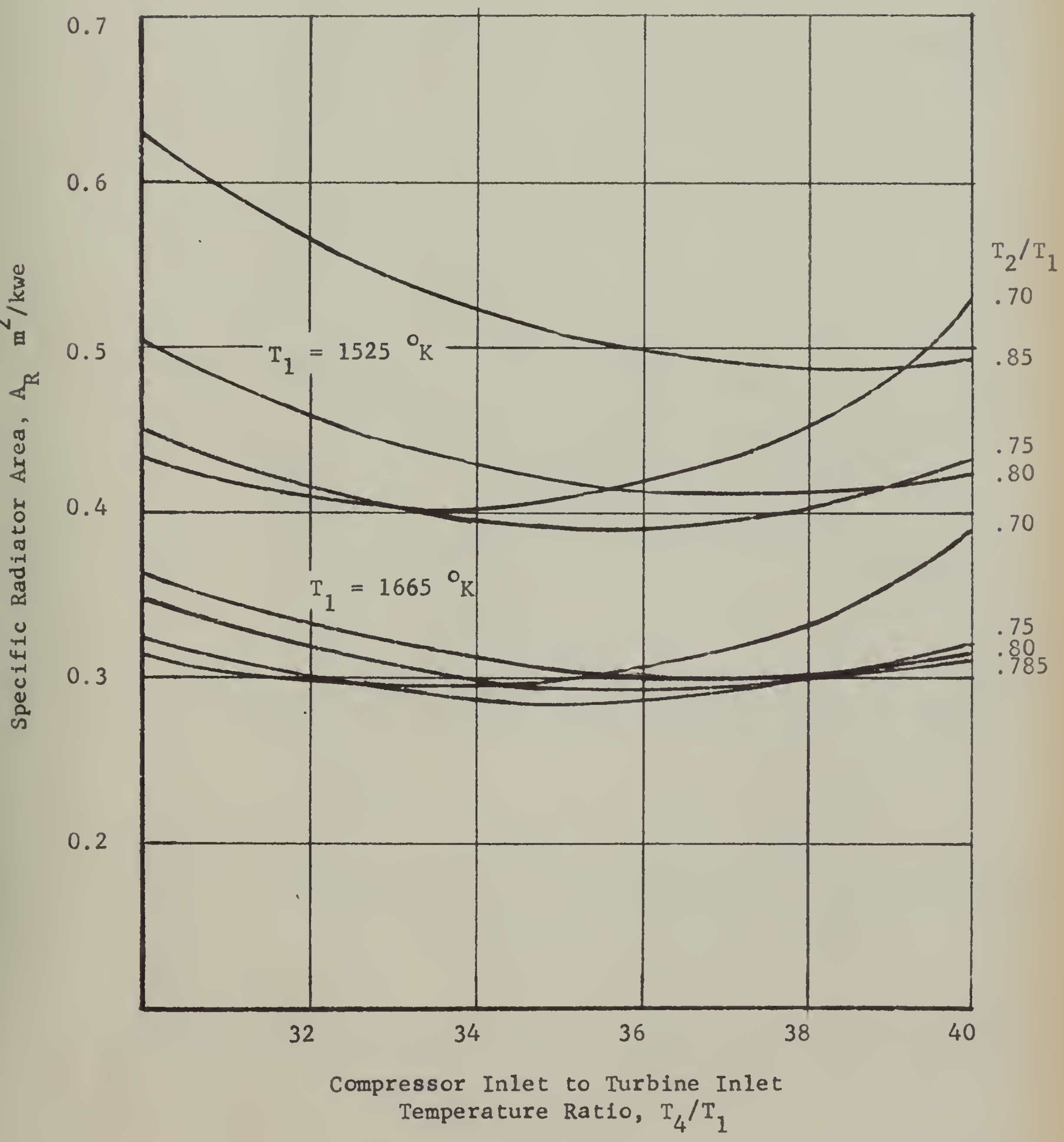

FIGURE 10

BRAYTON CYCLE

Specific Radiator Area
vs
Compressor Inlet to Turbine Inlet
Temperature Ratio

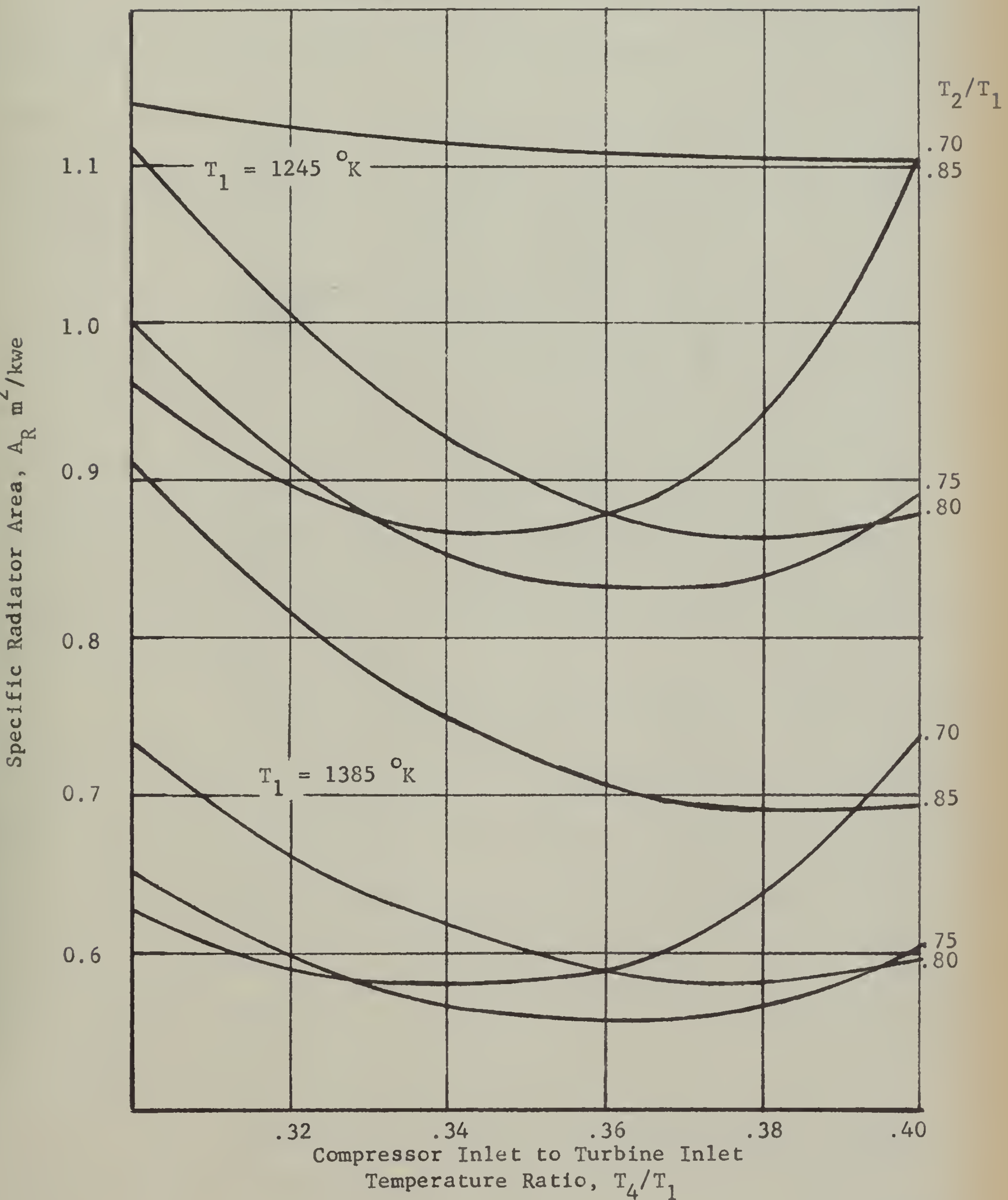

FIGURE 11

A similar analysis was made for turbine inlet temperatures of 1528°K, 1388°K and 1250°K using the same component efficiencies and temperature ratios. The results are recorded in Table IV and presented graphically in Figures 10 and 11. In each case the optimum cycle is obtained with a turbine temperature ratio, $T_2/T_1 = 0.35$. The corresponding required radiator areas increase with increasing turbine inlet temperature as would be expected. These results are similar to the results of the analysis in Reference 22. The Brayton cycle considered in Reference 22 used different component efficiencies and a different turbine inlet temperature. The optimum cycle for the case considered turned out to have a turbine temperature ratio, $T_2/T_1 = 0.75$, and a cycle temperature ratio, $T_4/T_1 = 0.30$.

Based on the figures generated in all of these studies, it would appear that the optimum Brayton cycle would have a turbine temperature ratio near 0.75 and a cycle temperature ratio, which is dependent on the cycle component efficiencies, having a value between 0.30 and 0.35. Each Brayton cycle should, therefore, be optimized as was done in this case to obtain a minimum mass system.

Having established the thermodynamic characteristics of the Brayton cycle to be used in the powerplant,

the next step is to consider the various components in the cycle and estimate their size and mass. Special attention was given to the reactor, shield and the radiator because of the significant size and mass of these components. A description of the cycle components and the methods used to size and determine their mass is given in the following paragraphs.

4. Component Masses

a. Reactor

The reactor concept chosen for the Brayton cycle is a homogeneous, gas-cooled, moderated reactor based on Pluto technology. (Reference 28). The feasibility of this type of reactor has been proven in the Tory II-A and Tory II-C test reactors. Although the concept was developed for use in a nuclear ramjet requiring large amounts of power, it is felt that it can be easily adapted to the closed-gas loop nuclear electric Brayton cycle.

The original decision to develop a moderated reactor for the nuclear ramjet was based heavily on economic considerations. A fast reactor in general will require considerably more fuel for any reasonable size missile and hence will be more costly to operate. Although the cost is not as critical in the smaller reactor sizes being considered here,

and although fast reactors are generally a little lighter than moderated reactors, the homogeneous moderated reactor was selected primarily because of the successful state of the art achieved in the Pluto program. Heterogeneous gas core reactors have not been considered because of the difficulties encountered with cladding at the high reactor temperatures required.

The choice of materials for the type of reactor is somewhat limited. As is pointed out in Reference 28, to be a good moderator implies an element whose atoms are as close as possible to a neutron in mass. Counting out lithium and boron because they also capture the neutrons, this leaves only hydrogen, beryllium and carbon. The metallic hydrides that are popular for moderator material in heterogeneous reactors generally have maximum useful temperatures too low for use in the homogeneous core. Although certain of the carbides are suitable for the application, BeO is considered adequate for the working fluid concerned and a superior moderator for compact reactors.

Of the fuel materials presently considered, three appear the most promising. (Reference 25). They are uranium nitride, uranium carbide and uranium dioxide. Of these, UO_2 is the better known and most often used compound.

Although the carbide and nitride have better qualities as far as uranium density and thermal conductivity are concerned, they are more difficult to fabricate and in general their status of development is far behind that of UO_2.

In view of the above consideration, the reactor materials selected are a homogeneous mixture of BeO and UO_2. It is felt that a VeO-UO_2 core can be made to withstand the temperatures required for the Brayton cycle selected in this analysis. The scope of this work precludes a detailed design of the reactor. However, in order to estimate the mass of the reactor more accurately, and to have a reasonable estimate of the reactor constants upon which to base the shielding calculations, a model reactor has been proposed. This model is considered to be representative of the manner in which the Pluto technology can be extended to nuclear electric powerplant use. The volume fraction of the model reactor is as follows:

Material	Volume Percent
BeO	50.0
Fuel and Structure	20.0
Void	30.0
Total	100.0

In addition, a power density of 2 mwt/ft^3 was selected to determine the subject reactors diameters listed in Table V.

To determine the critical mass for the model reactor, a modified one group-age diffusion method was employed to the bare reactor as derived in Appendix D. All equations and the necessary group constants were obtained from Reference 29. The required mass of uranium for a $k_{eff} = 1.2$ was found to be 14.2 kg. The fuel burnup for 10,000 hours is estimated at 2 kg, well above the critical mass of the 4.87 mwt reactor considered. Although a 5 cm BeO reflector is installed around the core, the reflector savings are neglected for the pusposes of this analysis.

The masses of the subject reactor have been estimated on the basis of the volume fractions of the core, a 5 cm BeO reflector around the reactor, a 7.67 cm reflector between the reactor and shield, and a pressure vessel surrounding the reactor. The resultant masses are presented in Table VI.

b. Turbomachinery and Generator

The characteristics of high temperature turbine machinery for Brayton cycles is discussed in Reference 22. From the consideration therein, an axial flow tungsten turbine of seven or eight stages is considered necessary for the selected cycles. The turbine blade tip diameter required for the characteristics of the selected 1 mw cycle is given as

TABLE VI

Brayton Cycle

Powerplant Mass Breakdown

Generator Output Power (kwe)	500	1000	1500
Reactor			
Reactor Mass	280	414	550
Power Conversion System			
Turbine	160	324	490
Compressor	148	300	453
Generator	202	388	609
Recuperator	352	703	1057
Pressurizer and Valves	20	40	60
Piping	69	138	207
Controls	68	68	68
Containment Tank	78	150	225
Power Conversion System Mass (kg)	1097	2111	3169
Radiator			
Primary	351	703	1051
Secondary	15	28	41
Feed and Return	25	71	133
Radiator Mass (kg)	391	802	1225

Total Powerplant Mass (kg)	1768	3327	4944
Powerplant Specific Mass (kg/kwe)	3.54	3.33	3.29

approximately 25.4 cm. The dimensions for the turbines at the other power levels were scaled in the same manner as done for the turbomachinery in the Rankine cycle, namely, the turbomachinery diameter is proportional to the square root of power. The mass of the tungsten turbine was estimated by multiplying the mass of a similar sized molybdenum turbine, as used in the Rankine cycle, by the density ratio of the two materials concerned.

The mass of the multi-stage compressors was estimated by assuming a specific mass approximately equal to that of the molybdenum turbine designs. The generators were sized based on the same formula used in the Rankine cycle analysis and hence have the same masses. The individual component masses for the Brayton cycle turbomachinery and generators are listed separately and summed in Table VI.

The achiement of the high-temperature turbine technology assumed in this report, although not yet proven by actual development, is considered reasonable in light of the advancements by the gas turbine industry in general. The 1665°K turbine inlet temperature is certainly near the upper limit for uncooled gas turbines of the future, but with some of the new high stress tungsten alloys that are being developed, as described in Reference 24, the turbine performance required

in this cycle is believed to be entirely possible by the 1975-1985 time period.

c. Radiator

Since the radiator is usually the largest and heaviest component in the Brayton cycle, it was decided not to limit the radiator design to a particular missile configuration or to require the structural strength necessary to withstand launching. In this case the radiator would, of course, have to be carried into low Earth orbit in sections and assembled there before departing for Mars. Such a scheme seems practical for a propulsion system using a gas working fluid whereas it would be impractical for a system using a liquid metal working fluid.

When the launching constraints on radiator design are removed, a flat panel radiator configuration becomes desirable because it presents the most effective radiating area for a given panel plan area. A fin and tube design, although requiring a larger panel area than an unfinned radiator, offers considerable mass savings as pointed out in Reference 30. The savings in mass is the result of using light unarmored fins versus much heavier tubes requiring a heavy layer of armor to provide meteroid protection. Accordingly, a flat panel fin and tube radiator design fabricated from beryllium was selected

for the Brayton cycle powerplant.

In a fin and tube radiator design, as the panel area is increased the mass of the radiator decreases to a minimum and then increases as shown in Reference 30. The minimum mass radiator occurs where the reduction in the required tube area and the resulting mass of the tube armor no longer offsets the mass increase due to the decreased fin effectiveness. The optimization of the radiator design then requires a heat transfer analysis of the tube and fin panels for various fin widths to determine the area of the panels required to radiate the specified heat load. With the area fixed, the mass of the radiator panel can be determined and plotted as a function of the tube length or fin width to obtain the minimum mass radiator. The required analysis is outlined in the following paragraphs using the method given in Reference 31.

The analysis takes into account the temperature drop between the gas and the radiator tube, but neglects the small effect of a sink temperature in space. Using a set of coordinate axes with the x-direction down the length of the tube and the y-direction perpendicular to the tube, the steady state heat balance of a strip of tube and fin area of differential width, dy , leads to the equation,

$$\frac{w}{2} c_p \, dt = -\sigma\epsilon \left[F_t T_{wy}^4 \left(\frac{\pi D}{2} - t_f \right) + \int_{D/2}^{\frac{B+D}{2}} F_f T_{xy} \, dx \right] dy \tag{19}$$

where the gas temperature and wall temperature are related by,

$$T = \frac{\sigma\epsilon}{h_R} T_w^4 + T_w \tag{20}$$

For given constant values of the tube and fin view factors, $F_t = 0.85$ and $F_f = 0.90$, obtained from the plot in Reference 31, equation (19) can be integrated to yield,

$$NL \left[(\pi D - 2t_f) F_t + fB \right] = \frac{w_{cp}}{3\sigma\epsilon} \left[\frac{1}{T_{w_4}^3} - \frac{1}{T_{w_3}^3} \right] = A_R \tag{21}$$

where the product of the fin effectiveness, f , and fin width, B , is defined as

$$fB \equiv 2 \int_{D/2}^{\frac{B+D}{2}} F_f T_{xm}^4 \, dy \Big/ T_{wm}^4 \tag{22}$$

which is evaluated at the fourth root of the mean fourth power of the tube wall temperature; i.e.,

$$T_{wm} = \left(\frac{T_{w_4}^4 + T_{w_3}^4}{2} \right)^{\frac{1}{4}}, \tag{23}$$

Evaluating the fin effectiveness at T_{wm} and considering it constant for the length of the tube gives sufficient accuracy and conservative results when compared with an incremental

method as stated in Reference 31. Equation (22) can now be integrated using the differential equation controlling the steady state heat flow of the volumetric element, tdxdy , to relate dT_{xm} to dX , to obtain the result,

$$fB = \frac{1}{T_{wm}} \sqrt{.288 \frac{kt}{\sigma t} \left(T_{wm}^{5} - T_{cm}^{5}\right)} \qquad (24)$$

The length of the fin as a function of the temperature at the center of the fin, T_{cm} , can be obtained from the plots in Reference 31. Thus, for a given mid-fin temperature, the geometry of the required radiator panel is determined by the fin width, B , and the tube length, L , calculated from equation (21).

To increase system reliability it was decided to divide the radiator into several panels, each separated from the rest of the system by a valve which could be closed in the event of meteroid damage to the panel. Each panel can then be treated as a separate entity and since the exposed tube area of a panel is considerably less than for the whole system, much less meteroid armor thickness is required. The design radiator panel was sized using one-ninth of the required radiator area for the one-megawatt powerplant. The proper number of these panels can then be used for each of the three power levels.

A low mass flow rate per unit area of 245 kg/m^2 was selected to obtain a reasonably small pressure drop of 0.80 kg/cm^2 through the radiator. This mass flow rate per unit area is on the same order as the value used in the radiator design in Reference 25. An inside tube diameter of 0.95 cm (3/8 in) was chosen on the basis of the information in Reference 30, which shows this to be the optimum tube diameter. The required number of tubes for the design radiator panel was then determined to be 84, based on the design panel mass flow rate which is one-ninth of the required mass flow rate for the one-megawatt powerplant.

The corresponding heat transfer coefficient for turbulent flow calculated from the relationship,

$$h_R = 3.12 \times 10^{-5} \frac{k}{D} \left(\frac{DG}{\mu}\right)^{0.8} P_r^{1/3} \qquad (25)$$

was determined to be .286 kcal/sec m^2 $^{\circ}K$. It should be noted that this value is about four times as large as the heat transfer coefficient used in the Brayton cycle optimization analysis. The original value was selected in the early phases of the investigation based on a low mass flow rate per unit area to obtain a small pressure drop in the radiator. Subsequent calculations in the radiator design indicated a larger mass flow rate per unit area and thus a larger heat transfer coefficient

could be used. The larger heat transfer coefficient should have little effect on the Brayton cycle optimization, but will considerably reduce the required radiator area as seen by comparing the figures in Tables IV and V.

With the heat transfer coefficient thus determined, equation (20) was solved by iteration to obtain the tube wall temperature at the radiator inlet, T_{w_3}, and outlet, T_{w_4}. These values were then used in equation (21) with the required design panel mass flow rate to determine the effective panel radiator area of 25.3 m^2. The mean fourth power of the tube wall temperature was established using equation (23).

Three fin thicknesses of .0381 cm, .0762 cm and .1144 cm were selected to examine the effect of fin thickness on the radiator design. Having now determined all of the values in equations (21) and (24) except the design radiator panel tube length and the temperature at the center of the fin, the tube length was calculated for various assumed values of the mid-fin temperature. The fin width obtained from the curve in Reference 31 fixed the dimensions of the design radiator panel. The required beryllium armor thickness for a 95 percent non-puncture probability for 10,000 hours was obtained from the plots in Reference 14. The masses of the armored tubes, and headers, and the fins were then computed

using the calculated dimensions and the density of beryllium of 1.85 gm/cm^3 to obtain the mass of each panel.

Panel design mass was then plotted as a function of tube length and the parameter fin thickness in Figure 12. From Figure 12, the optimum radiator panel design has a fin thickness of .0762 cm, and a tube length of 2.84 m with the corresponding fin width of 4.52 cm. The design radiator panel with allowance for headers is 3 meters long and 5.12 meters wide and has a mass of 78 kg.

It is interesting to note that an increase or decrease in the fin thickness from the .0762 cm value produces a radiator of greater mass as shown in Figure 12. Apparently, the design with a .0381 cm fin thickness has a less efficient fin resulting in an increase in the mass of the radiator and the design with a 0.1144 cm fin thickness uses fins which are too heavy which also results in an increase in the mass of the radiator.

The required primary radiator area and the radiator area required to cool the generator were obtained for each power level using equation (21). The number of panels and thus the mass of the radiator was obtained by dividing these areas by the effective radiator area of the design panel; i.e., 25.3 m^2. The resulting radiator masses are listed in Table VI.

BRAYTON CYCLE

Radiator Panel Mass vs Tube Length

Panel Area = 25.3 m^2
Tube I.D. = 0.953 cm
Fin Thickness, t_f = .0382, .0764 and .1145 cm

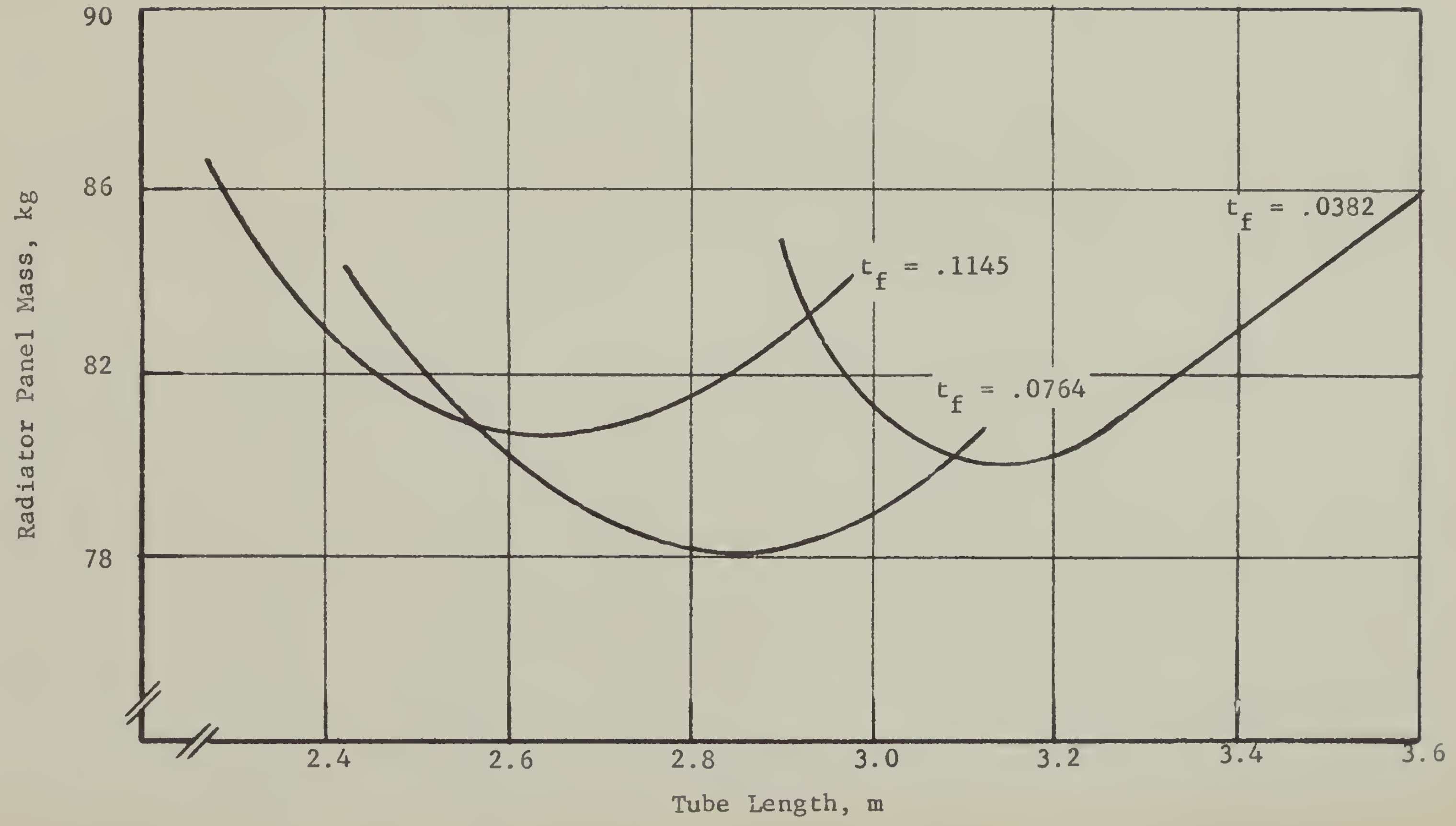

FIGURE 12

d. Recuperator

The recuperator for the Brayton cycle powerplant is a plate and fin type heat exchanger fabricated out of stainless steel. It is a counter-flow heat exchanger with triangular shaped passages like the one designed for the 100 kwe Brayton cycle space powerplant contained in Reference 25. The recuperator was sized by determining the required heat transfer area based on the heat powers and mass flow rates in Table V using the formula,

$$\frac{GQ}{w} = \frac{Q}{A} = \frac{T_h - T_c}{\frac{1}{h_h} + \frac{1}{h_c}} \tag{26}$$

The temperature drop in the recuperator is 64°K, the mass flow rate per unit area was taken as 245 $kg/m^2 sec$ and the corresponding heat coefficient was calculated to be 0.273 $kcal/m^2 sec\ {}^oK$ using equation (25). Values of the required recuperator heat transfer area are recorded in Table V.

The mass of the recuperator was determined by scaling the recuperator design in Reference 25 to the required size. The mass per unit of heat transfer area for this design was computed to be 2.6 kg/m^2. This figure was multiplied by the ratio of the recuperator inlet pressure in the Brayton cycle powerplant to the inlet pressure for the recuperator design in Reference 25 to account for the higher pressures.

This scale factor was arrived at on the basis that the passage wall thickness is proportional to the pressure and the mass of the recuperator is proportional to the wall thickness. The resulting mass per unit of heat transfer area of 9 kg/m^2 was then multiplied by the required heat transfer area to obtain the recuperator masses listed in Table VI. The pressure drop in the recuperator was taken as 0.11 kg/cm^2 based on the design data of the recuperator in Reference 25.

e. Piping and Associated Equipment

The piping, valves and powerplant controls used in the Brayton cycle powerplant were assumed to have the same mass allowed for similar items in the liquid metal Rankine cycle. The mass of the working fluid pressurizer was taken as 40 kg for the 1000 kwe powerplant and scaled on mass flow rate for the other powerplants. A cylindrical vessel is used to enclose the power conversion equipment similar to the scheme used in the liquid metal Rankine cycle powerplant. The mass of this structure was scaled from the data in Reference 14 proportional to the mass of the components inside the containment vessel. A complete mass breakdown of all the components in the Brayton cycle is presented in Table VI.

The resultant powerplant specific masses for the Brayton cycle are: $\propto_{pp}$ = 3.54 kg/kwe at 500 kwe,

α_{pp} = 3.33 kg/kwe at 1000 kwe and α_{pp} = 3.29 kg/kwe at 1500 kwe. Curves of powerplant specific mass, α_{pp}, versus powerplant output in electrical energy are plotted in Figure 13 for both liquid metal Rankine cycle and the Brayton cycle.

Nuclear Turboelectric Powerplant Specific Mass
vs
Power Output

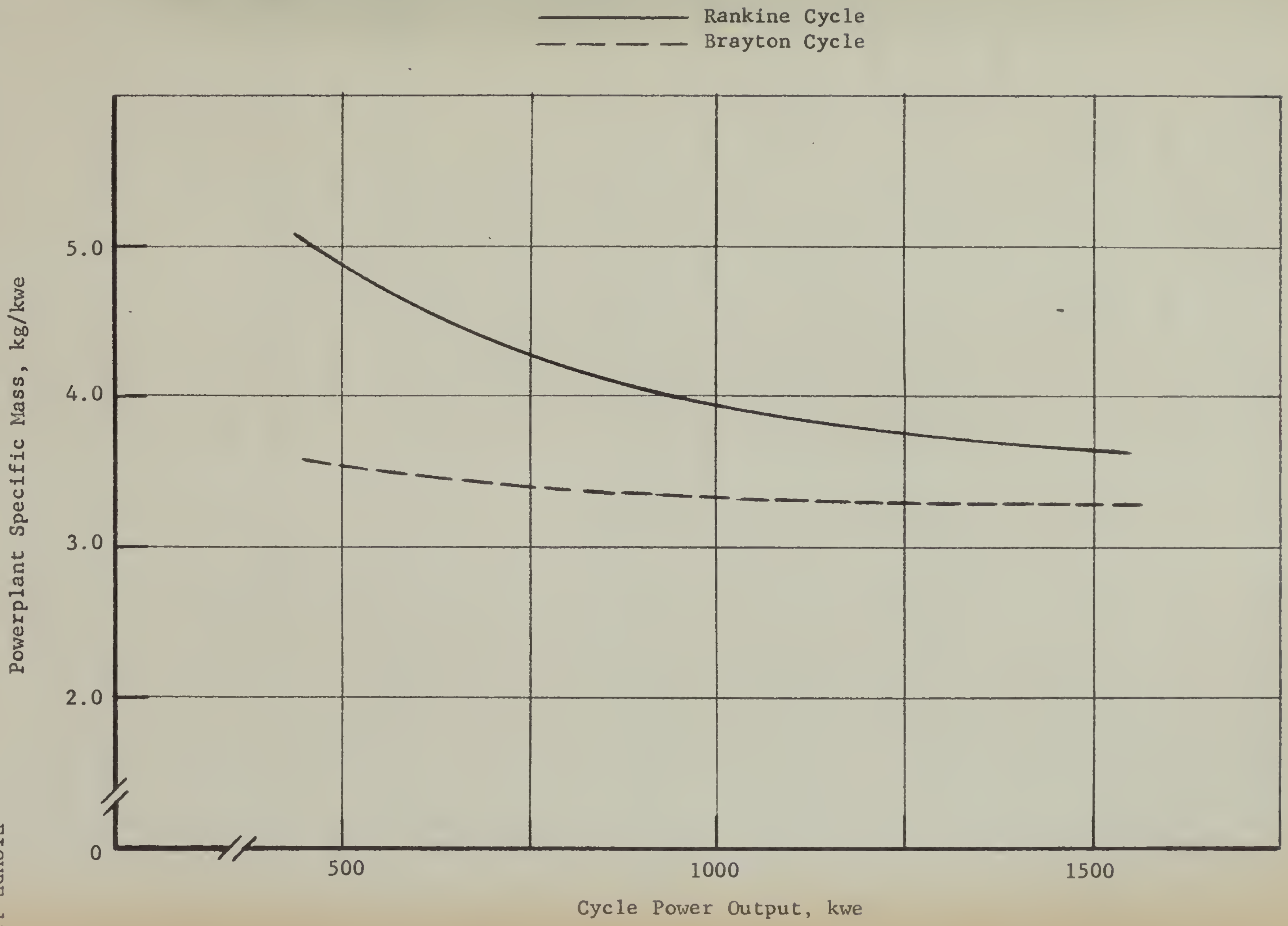

FIGURE 13

IV. SPACECRAFT FOR THE UNMANNED MARS ROUND TRIP MISSION

A. Spacecraft Components

The basic vehicle concepts envisioned for the round trip to Mars are similar for both the liquid metal Rankine and the Brayton cycle powerplants with one major exception, the radiator. The spacecraft using the Rankine cycle powerplant employs a truncated cone-shaped radiator and the Brayton cycle spacecraft uses a flat plate radiator. The radiator configuration causes a heavier reactor shield on the Rankine cycle vehicle and a longer overall Brayton cycle vehicle, otherwise the two vehicles are almost identical.

In the following paragraphs, a more detailed description will be given of the major vehicle components.

1. Reactor Shields

The amount of shielding required for a nuclear electric spacecraft is determined by the components that have the least radiation tolerance. In the subject vehicle these components are considered to be the payload itself (the Mars samplings) and the various electronic components required for guidance and control of the spacecraft and excursion vehicle. For the purpose of the shielding analysis, these components will all be considered as located in one payload compartment near the aft end of the spacecraft.

The allowable dose for typical payload electronics has not been accurately determined. From recently available reports, Reference 14 and Reference 25, a value of 10^6 rads of gamma rays and 10^{11} nvt of fast neutrons seems to be a conservative estimate. The allowable dose for the Mars samplings will not be considered here except to note that additional local shielding may be required around the sample cannisters themselves. Therefore, for this analysis the allowable payload dose is considered to be 10^6 rads of gamma rays and 10^{11} nvt of fast neutrons for the 10,000 hour design period. An additional requirement of 5×10^7 rads of gamma rays has also been imposed on the power conversion equipment located directly behind the shield. Since there will be no allowance made for the shielding effect of the power conversion containment vessel and the shielding effect of other equipment within the vessel, the actual dose received by any one piece of power conversion equipment should be considerably less than the allowable dose.

The problem of reactor shielding can be broken up into three phases, the slowing down of fast neutrons, the capture of slow neutrons and the attenuation of gamma rays. Elements with reasonably high mass numbers are generally selected for the initial slowing down of fast neutrons because they

reduce the neutron energy by inelastic scattering collisions. Once the neutron has been slowed down to an energy of 1 mev or less, the scattering cross section of lighter elements such as hydrogen become significant and are very effective in continuing the slowing down process. Therefore, the combination of both a heavy and a light element in a shield presents a very effective means of slowing down fast neutrons.

The capture of the neutrons, once they have slowed, is accomplished with relative ease by hydrogenous materials. Although the capture cross section of hydrogen is not too large for thermal neutrons, there is generally a sufficient number of hydrogen nuclei present that the capturing of the neutrons is fairly certain. Gamma rays, regardless of their origin, are best attenuated by substances with high linear attenuation coefficients and these are generally the elements with high density.

Accordingly, from the previous considerations, the shielding materials chosen for this analysis were tungsten and lithium hydride. In the previous section on reactor design, it was determined that this reactor was well down in the thermal region and hence the fast neutrons do not dominate shielding considerations in the case studied here. In addition, there is a three inch (7.62 cm) beryllia reflector between the reactor core and the front face of the shield which

acts as an excellent moderator to the fast neutrons escaping from the core. Because of this, only a thin layer (1 cm) of tungsten is needed on the front face of the shield to stop the fast neutrons and to act as a cladding for the lithium hydride. The remainder of the tungsten, for the majority of the gamma ray attenuation, is placed last in the shield where the secondary gamma ray emission from fast neutrons will be minimized.

The values of the removal cross section, attenuation coefficients and densities of the various materials used in this analysis are given in Table VII. The removal cross sections were obtained from Reference 32 and the attenuation coefficients from Reference 32 and Reference 33. In determining the total removal cross section for the core, the individual microscopic cross sections for BeO and UO_2 were corrected for core temperature by the well known expression:

$$\sigma_{eff} = \sigma_{(2200)} \sqrt{\frac{T_{293\ ^{o}K}}{T_{core}}} \times \frac{\sqrt{\pi}}{2} \qquad (27)$$

Numerous calculations were made to determine the thicknesses of lithium hydride and tungsten that produced the minimum mass and still reduced the gamma and neutron flux to an acceptable level. To allow for scattered and secondary radiation, the allowable primary dose was reduced by fifty

TABLE VII

Brayton Cycle

Shielding Criteria and Resultant Dose Rate

Material	Density (g/cm^3)	σ_R (barns)	$\overline{\Sigma}_r$ (cm^{-1})	μ_a (cm^2/g)	μ_a (cm^{-1})
W	19.3	3.36	.212		.554
Li	0.534	1.01	.116		
H	8.9×10^{-5}	1.00			
LiH	.79		.120		.028
Be	1.85	1.07		.0313	
O	.0014	0.99		.0359	
U	18.9	3.6		.0445	
BeO	3.025		.150*	.0343	.1046
UO_2	10.0		.135*	.0404	.4040
CORE			.0377		.1331

*Corrected for core temperature.

Shield Material Thicknesses

1 cm W	110 cm LiH	4.2 cm W

Existing Dose Rate

Dose	Power Conversion Compartment	Payload
Gamma, rads	2.47×10^{7}	5.75×10^{3}
Neutron, nvt	2.19×10^{12}	1.275×10^{10}

percent. For the gamma source it was assumed that five 3 mev particles were emitted per fission. From Reference 32, for a 3 mev photon, 1 rad/hr = 7.89×10^5 mev/cm^2-sec, hence, the maximum permissible flux in the middle of the power conversion equipment (i.e., 3 meters from the reactor) is 1.97×10^9 mev/cm^2 sec. The maximum allowable flux at the payload is 7.89×10^7 mev/cm^2-sec. Likewise, the allowable neutron flux of 10^{11} nvt becomes 2.78×10^3/cm^2-sec.

The equation for determining the flux from a cylindrical source was obtained from Reference 34 and is,

$$\phi = \frac{B_1 S_v}{2 \mu_s} \left[E_2(b_1) - \frac{E_2(b_1 \sec \theta)}{\sec \theta} \right] \qquad (28)$$

For neutrons, assuming 2.5 neutrons per fission in U_{235} , the source term, S_v , is given by Reference 29 as

$$S_v = 7.8 \times 10^{10} \ \frac{P}{V} \ \text{neutrons/cm}^3 \text{ sec}$$

The term μ_s is the total removal cross section of the core and the buildup factor, B_1 , is used to compensate for the heavy material following the hydrogenous material as in Reference 35. For the gamma flux, the term μ_s is the total linear attenuation coefficient for the core and the buildup factors were obtained directly from Reference 33. In both cases, the quantity b_1 is the summation of $\mu_1 t_1$ for the

shield material and $E_2(b_1)$ are integrals evaluated from the graphs in Reference 34.

A distance of 1.5 meters from the reactor core was chosen for the initial flux calculations in order that the value of secant θ would be sufficiently large to enable relative accurate interpretation of the graph of Reference 34. The flux at a distance of 3 meters and at the payload were considered to be inversely proportional to the square of the distance. In addition, the payload gamma flux was reduced by a factor of 100 because of the shadow effects of the power conversion equipment, as is considered in Reference 14. The resultant dose values for the 1 mwe shield are presented in Table VII.

Since the power densities of the reactors in this analysis are constant, the radiation fluxes of the 500 kwe and 1.5 mwe reactors will remain the same except for the small correction to secant θ due to the changing core diameter. Accordingly, the shield thickness is considered constant for all three vehicles and hence the total shield mass will be taken as constant since the shielding cone angle for all three vehicles is essentially the same.

The geometrical shape of the reactor shadow shield in the Brayton cycle vehicle is shown in Figure 14. It

BRAYTON CYCLE

Reactor Shield for 1 Mwe Spacecraft

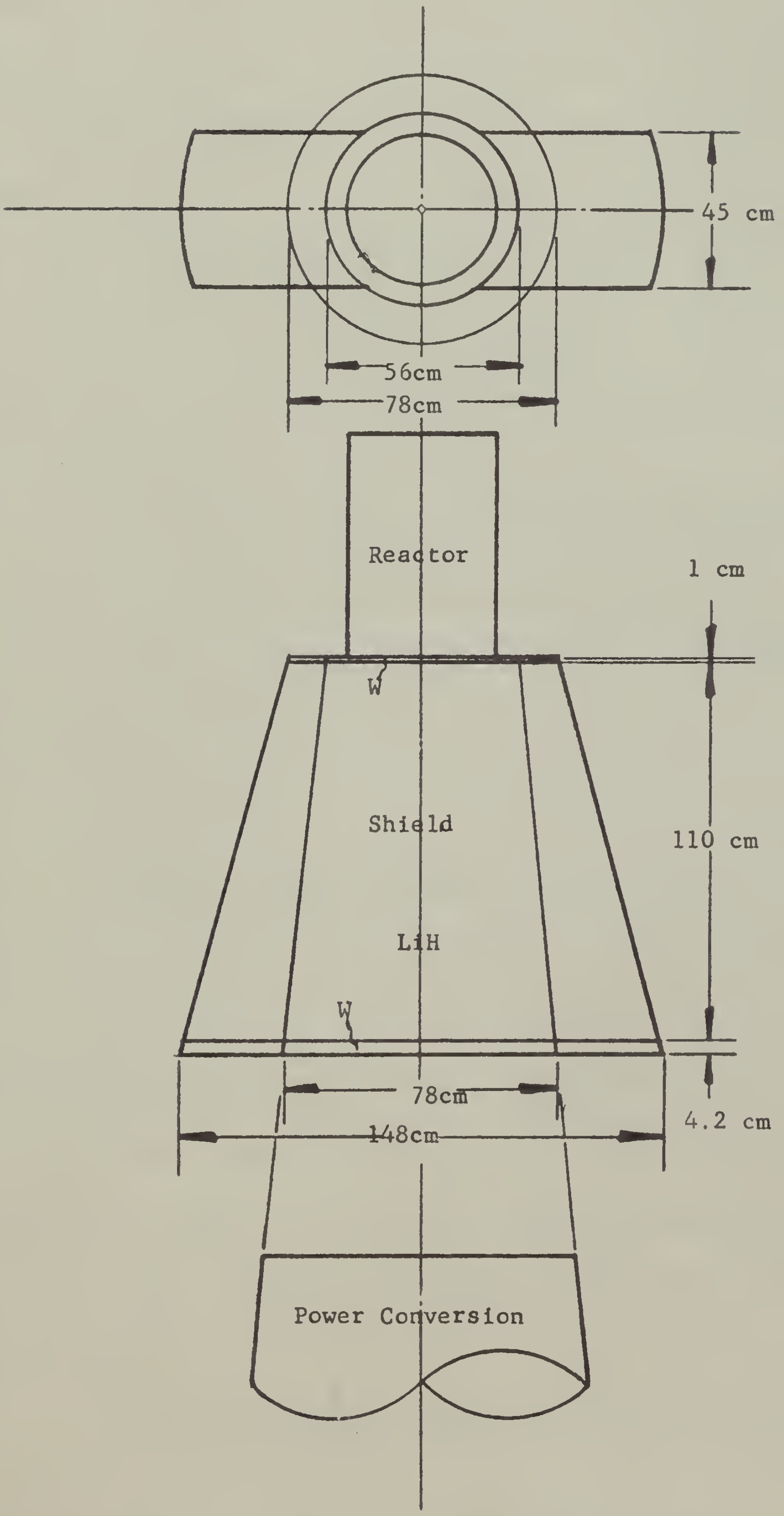

FIGURE 14

is obvious that the total mass is less than that of the truncated cone, since a smaller area need be shielded. It is noted that the payload shielding requirements are essentially the same in both vehicles, it is only the scatter shielding requirements as dictated by the radiator configurations that change. The total mass of the reactor shadow shield for the Brayton cycle vehicle, therefore, using the shield cross section developed earlier and presented in Table VII, was calculated to be 1097 kg.

The reactor shadow shield for the Rankine cycle vehicle is a truncated cone with a centerline cross section identical to that presented in Reference 14. The mass of the shield was estimated as 1559 kg.

2. Thrusters

Magneto plasma dynamic arc jets were selected as the thrusters to propel the spacecraft, since they represent one of the most practical recent propulsion schemes in the characteristic velocity and thrust ranges suitable for the selected mission. These thrusters use a high current arc in a low pressure chamber to heat the hydrogen propellant. The propellant is then expanded through a nozzle to produce the required thrust.

Private communications with Dr. R. R. John at the

TABLE VIII

Liquid Metal Rankine Cycle

Spacecraft Mass Breakdown

Generator Power Output (kwe)	500	1000	1500
Powerplant			
Reactor	459	665	808
Power Conversion System	886	1,570	2,248
Radiator	1,097	1,711	2,395
Powerplant Mass (kg)	2,242	3,946	5,451
Powerplant Specific Mass (kg/kwe)	4.89	3.95	3.64
Propulsion System			
Powerplant	2,242	3,946	5,451
Shield	1,559	1,559	1,559
Thrusters, Power Conditioning, Controls and Thruster Radiator	1,136	2,270	3,410
Electrical Transmission Lines	52	115	169
Propulsion System Mass (kg)	4,989	7,890	10,589
Propulsion System Specific Mass (kg/kwe)	9.96	7.89	7.05
Spacecraft			
Propulsion System	4,989	7,890	10,589
Propellant Tanks	1,748	1,748	1,748
Payload, Tank and Thrust-Structure	1,650	1,705	1,762
Navigation, Guidance and Control	1,000	1,000	1,000
Spacecraft Mass (kg)	9,387	12,343	15,099
Spacecraft Specific Mass (kg/kwe)	18.77	12.34	10.06

Initial Mass in Low Earth Orbit			
Spacecraft	9,387	12,343	15,099
Propellant	21,000	21,000	21,000
Payload	9,115	9,115	9,115
Initial Mass (kg)	30,502	42,458	45,214

TABLE IX

Brayton Cycle

Spacecraft Mass Breakdown

Generator Power Output (kwe)	500	1000	1500
Powerplant			
Reactor	280	414	550
Power Conversion System	1,097	2,111	3,169
Radiator	391	802	1,225
Powerplant Masss (kg)	1,768	3,327	4,944
Powerplant Specific Mass (kg/kwe)	3.54	3.33	3.29
Propulsion System			
Powerplant	1,768	3,327	4,944
Shield	1,097	1,097	1,097
Thrusters, Power Conditioning Controls and Thruster Radiator	1,136	2,270	3,410
Electrical Transmission Lines	55	123	180
Propulsion System Mass (kg)	4,056	6,817	9,631
Propulsion System Specific Mass (kg/kwe)	8.11	6.82	6.42
Spacecraft			
Propulsion System	4,056	6,817	9,631
Propellant Tanks	1,748	1,748	1,748
Payload, Tank and Thrust Structure	1,650	1,705	1,762
Navigation, Guidance and Control	1,000	1,000	1,000
Spacecraft Mass (kg)	8,454	11,270	14,141
Spacecraft Specific Mass (kg/kwe)	16.90	11.27	9.43

Initial Mass in Low Earth Orbit			
Spacecraft	8,454	11,270	14,141
Propellant	21,000	21,000	21,000
Payload	9,115	9,115	9,115
Initial Mass (kg)	38,569	41,385	44,256

AVCO Research Laboratories indicate that the magneto plasma dynamic arc thrusters presently being investigated will have a specific mass of about 2.25 kg/kwe. This includes the mass of the thruster, cooling radiator and thruster controls as well as the mass of the power conditioning equipment to convert the generated 1000 volts a.c. to the 100 volts d.c. required by the thruster. The thrusters should be capable of thrusts from 3 to 150 n, characteristic velocities from 25 to 100 km/sec. and have efficiencies from 0.50 to 0.75.

The thrusters are supported by a light structure, the details of which are not considered here. A nominal estimate of the mass of the electrical feeders required to transmit the current to the power conditioning equipment and from there to the thrusters was obtained from the nomographs in Reference 14. The masses of the thrusters and associated equipment and the electrical transmission lines are recorded in Tables VIII and IX along with the masses of the rest of the components of the propulsion system. The corresponding propulsion system specific masses range from 6.42 to 9.96 kg/kwe as shown in Tables VIII and IX.

The mass of the structure required to support the propellant tanks, thrusters, power conditioning and guidance and control equipment was estimated at five percent of the mass

of these components. The mass of the navigation, guidance and control equipment was estimated at 1000 kg based on the mass of similar equipment used in the spacecraft design in Reference 14. The mass of each spacecraft component is listed in Tables VIII and IX. The resulting spacecraft specific masses range from 9.43 to 18.77 kg/kwe.

3. Propellant Tanks

The design of propellant tankage depends on the mission requirements and on the tank geometry. For the mission of interest in this analysis, the required propellant mass varies from 10,000 kg to 50,000 kg, dependent on the total trip time and spacecraft specific mass. Therefore, several tank masses have been computed over a range of values between these limits. The specific case of required propellant equal to 19,000 kg is presented here as an example of the methods used in making the calculations.

The required propellant mass in addition to that used for propulsion is presented in Table X. The hydrogen leakage and amount of propellant remaining in the tank at the completion of the mission came from considerations presented in Reference 36 where similar conditions were treated in more detail. The amount of hydrogen boiloff was estimated from data in Reference 35 and is considered reasonable for a well

insulated tank over the period of time required.

In calculating the required volume of tankage, five percent was allowed for ullage. The total volume, including both liquid and vapor, was found to be 310 m^3. To package the large volume in the conceivable boosters of the future, four cylindrical tanks with hemispherical heads were chosen. Each has a diameter of 3.96 m and an overall length dependent on the mass of propellant required. There are certain advantages accruing from having several tanks completely full of fuel for a large part of the mission. Also, the size of the individual tanks is more reasonable when handling and manufacturing aspects are considered.

The tanks are constructed out of annealed 5 Al - 2.5 Sn titanium alloy which has a tensile strength of 19,500 kg/cm^2 and a yield strength of 19,080 kg/cm^2 at the liquid hydrogen temperature. The construction of the tanks is similar to that presented in Reference 36 with a design pressure of 3.87 kg/cm^2; the thickness of the cylinder walls was selected at .046 cm and the hemispherical heads at .025 cm. The tank must have some internal pressures at all times to keep from collapsing. The mass of the tank was determined to be 167 kg for the selected case.

To provide meteroid protection, the thin bumper

concept is employed for a decrease in total mass over the concept of increasing the thickness of the tank walls. For this analysis, a 5 mil Mylar sheet has been used similar to that designed in Reference 36. To reduce the heat flux into the liquid hydrogen from space sources, an insulation blanket of the multi-foil radiations shield type is employed. This material is assumed to have a density of 8.02×10^{-5} kg/cm^3.

There are three other primary sources of heat flux into the hydrogen, nuclear radiation from the reactor and thermal radiation from both the radiator and guidance and control compartment. From the predicted dose level at the forward end of the tanks, the total heat load due to gamma radiation amounted to less than 3 watts per tank because of the large separation from the reactor.

Of much more significance is the heat load from the nearby space radiators. Using the view factors presented in Reference 36, the heat load from the radiators was calculated to be 63 kw per tank. This amount is considerably more than allowable and must be reduced by the use of thermal shadow shields. These shields are generally very light and their most effective use requires the stacking of several thin shields with relatively small spacing between them. From Reference 35, the mass of a typical shield is approximately .342 kg/m^2 plus the structural weight required for support.

A similar type of shield is required between the payload and the tanks although the heat flux created by the payload is considerably less than that generated by the radiator. Based on the above considerations, the total mass of thermal radiation shielding is estimated at 22 kg. for the selected case.

The various masses for a single tank are summed in Table X. Although these masses were derived from considerations of the 1 mwe vehicle, there will be very little difference in the total tank mass for all three vehicles requiring the same initial amount of propellant. Also, from the results of the other calculations, it has been determined that the total tank mass varies approximately as a linear function of required propellant mass. The resultant curve of total tank mass versus required propellant for the round trip Mars mission is plotted in Figure 15.

B. General Configuration

The one-megawatt vehicles are shown in Figures 16 and 17. The component masses for each spacecraft are listed in Tables VIII and IX. Both vehicles begin with the reactor foremost in the vehicle to minimize the required shielding angle and then are followed by the reactor shadow shield allowing sufficient space between the reactor and shield for fluid ducts

Total Tank Mass vs Total Propellant Mass

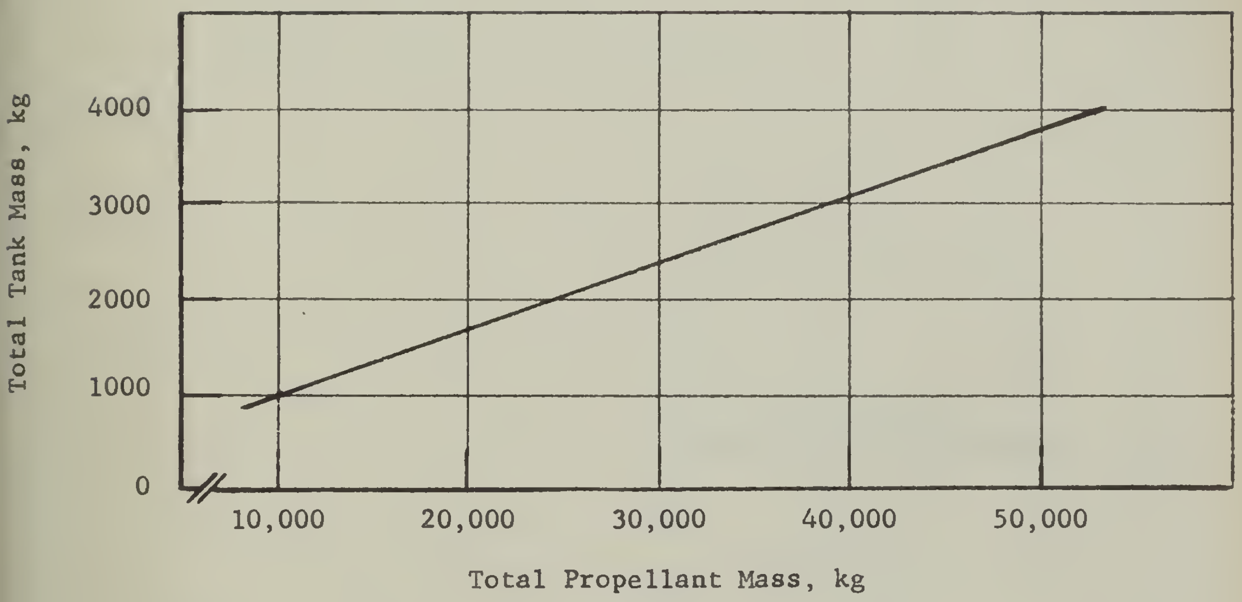

FIGURE 15

TABLE X

Tank and Propellant Masses

Item	Mass (kg)	Item	Mass (kg)
Propellant required	19,000	Tank	164
Usable reserve	950	Meteoroid	43
Left in tank	100	Insulation	168
Leakage	50	Shielding	22
		Misc Stru. & Piping	40
Total	21,000	Total	437 kg

Total tank mass = 1748 kg

RANKINE CYCLE

Nuclear Turboelectric One
Megawatt Spacecraft

Propellant mass = 21,000 kg
Specific mass, α_s = 12.34 kg/kwe

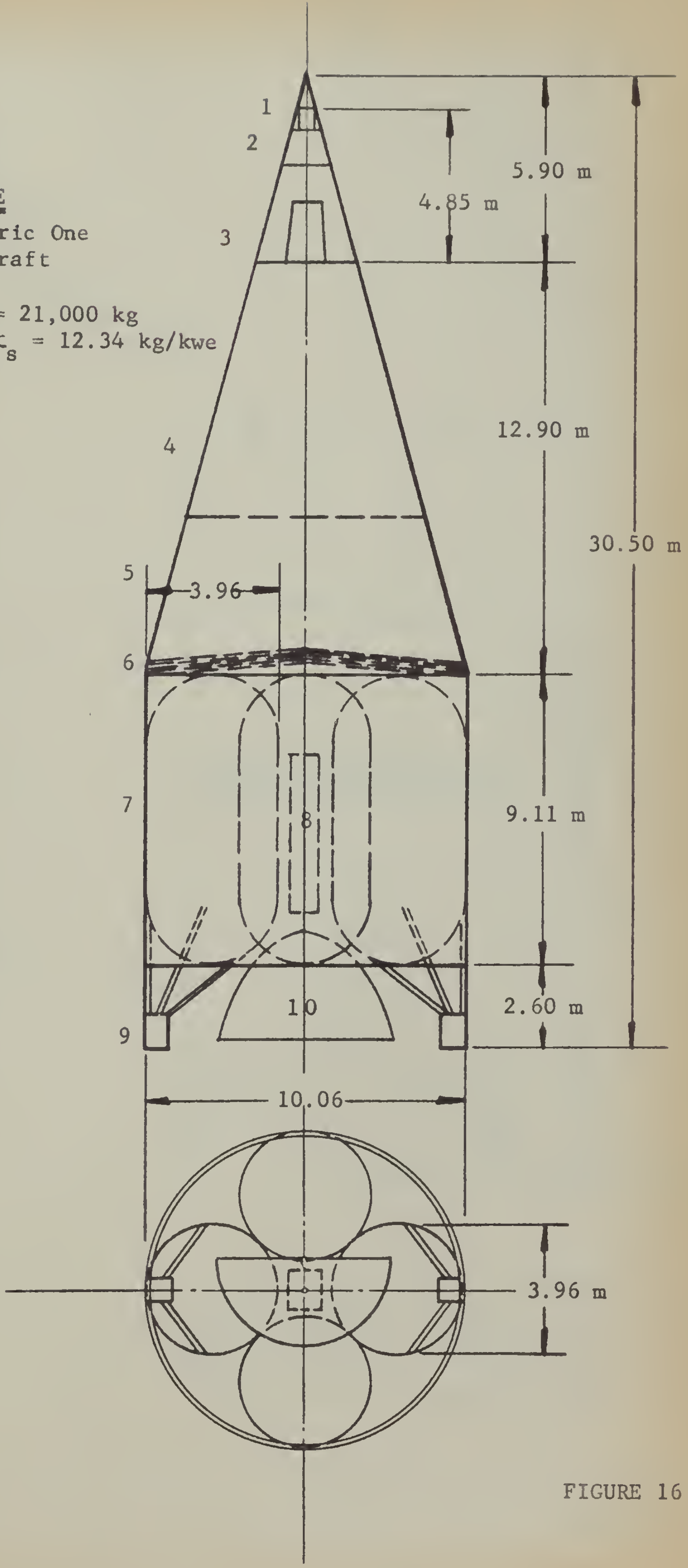

LEGEND:

1. Reactor
2. Shield
3. Power Conversion
4. Conical Radiator
5. Fairing
6. Thermal Shields
7. Tanks
8. Guidance & Control
9. Thrusters
10. Excursion Vehicle

FIGURE 16

BRAYTON CYCLE

Nuclear Turboelectric One
Megawatt Spacecraft

Propellant Mass = 21,000 kg
Specific Mass, α_s = 11.27 kg/kwe

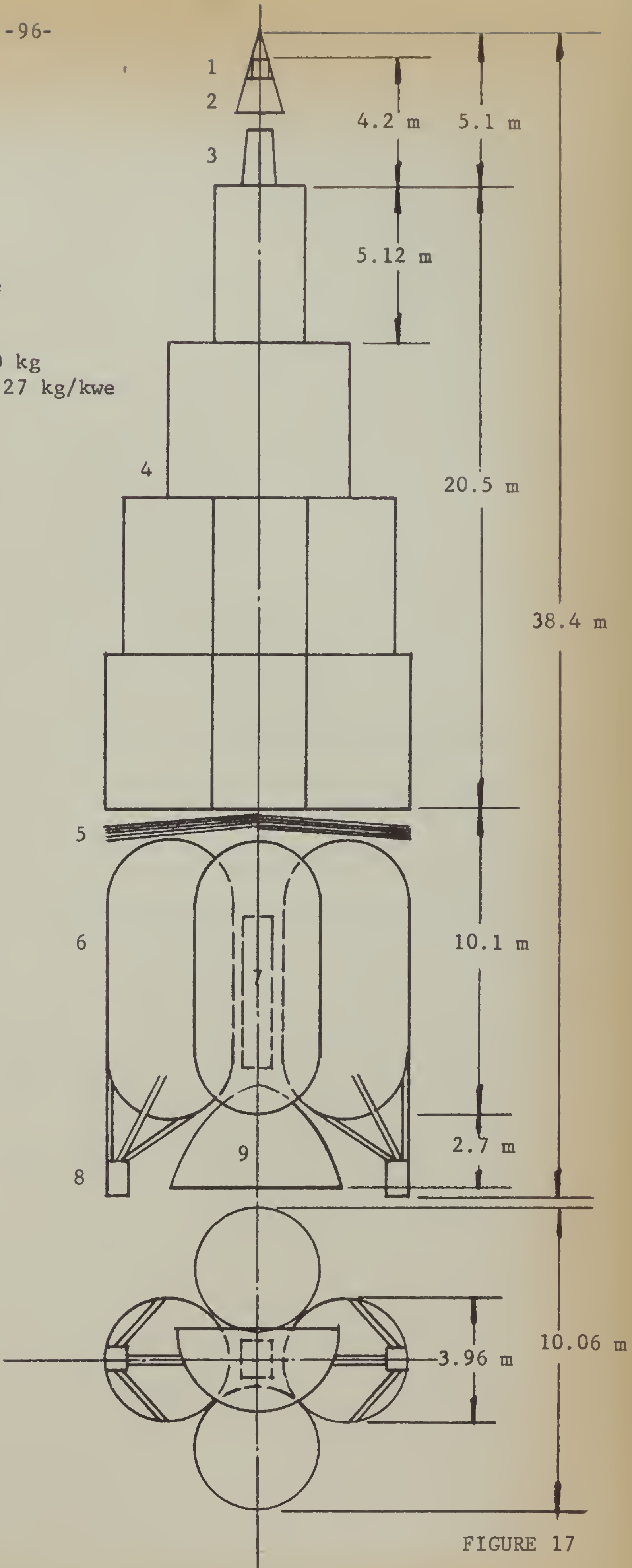

LEGEND:

1. Reactor
2. Shield
3. Power Conversion
4. Radiators
5. Thermal Shields
6. Tanks
7. Guidance and Control
8. Thrusters
9. Excursion Vehicle

FIGURE 17

and necessary reactor controls. Next is the power conversion containment vessel, the center of which is approximately three meters aft of the rear face of the reactor. The conical radiator on the Rankine cycle is a self-supported structure stressed for launch with the necessary feed pipes and power cables running through the center. The flat plate radiator of the Brayton cycle vehicle is made up of numerous panels which could be assembled in space or stressed for launch with a series of cables and other lightweight structure. The primary structure support on launch could come from the radiator feed pipes themselves which run the length of the radiator. Between the radiator and tanks are located the thermal shields which reduce the heat flux from the radiator. In between the tanks is located the guidance and control package which is approximately one meter square and can be any desired length up to seven meters. Aft of the tanks are the four thrusters, of which only two are shown in Figures 16 and 17 for clarity. Between the thrusters is nestled the excursion vehicle in the approximate shape as depicted in Reference 7.

V. DISCUSSION OF RESULTS

A. Powerplant

The plot in Figure 13 of powerplant specific mass versus cycle electrical output power for each of the cycles shows graphically the results of the powerplant analysis. The curves in Figure 13 indicate that the Brayton cycle powerplant compares very favorably with the reference liquid metal Rankine cycle powerplant at all of the power levels examined. The powerplant specific mass of the Brayton cycle with a 381°K higher turbine inlet temperature is actually less than that of the reference liquid metal Rankine cycle. In both cycles the specific powerplant mass decreases with increasing power level in the power range of 500 to 1500 kwe investigated. From the curves in Figure 13, it would appear that the powerplant specific mass levels out in the power range just beyond 1500 kwe.

The basic difference between the problems associated with the Rankine and Brayton cycles centers around the working fluids involved. In the Rankine cycle the liquid metal working fluid provides a system with good performance, but requiring containment and structural materials highly resistant to corrosion. The liquid metal Rankine cycle is limited to turbine inlet temperatures around 1300°K by the containment materials presently in use. Development of new materials

would require new research and development time and result in the additional expense involved.

In the Brayton cycle which uses an inert gas working fluid, the problem of compatibility with materials does not exist. Based on the generally good developmental history of closed loop gas cycles, it seems reasonable to predict that turbine inlet temperatures up to $1950^{o}K$ are probable in the near future if the required developmental work is performed. Gas turbines operating at these temperatures will probably have a somewhat lesser efficiency, but it is felt that turbines operating at temperatures as high as $1665^{o}K$ with a high efficiency can be developed for use in the Brayton cycle.

Powerplant starting considerations are also closely linked to the working fluid. The reference Rankine cycle powerplant would have to be preheated before the liquid metal is introduced into the system. This is a process which would probably be performed on the ground before launch and the powerplant started as soon as the spacecraft is safely in orbit and kept running to prevent the working fluid from freezing. To design the liquid metal Rankine cycle powerplant to be capable of shutting down during the coast phases of the mission and restarting would require the additional mass penalty of the preheating equipment.

Powerplant reliability is another problem of concern. The present aim is to demonstrate 10,000 hours of successful operation which is about 417 days. This would be near the minimum allowable reliability period for this mission if the powerplant was secured during the coast phases, since the mission will probably require 600 days or more. Succeeding missions will probably require trip times greater than this. System reliability can certainly be improved by duplication. Component reliability will still be a major factor and the use of a non-corrosive working fluid will help solve this problem.

Since the Rankine cycle and Brayton cycle powerplant specific masses are comparable with a reasonable increase in the Brayton cycle turbine inlet temperature, and in view of the various working fluid considerations above, it would seem that some research and development time should be given to further investigation of the Brayton cycle for use as a propulsion powerplant.

The major differences in the components of the Brayton cycle and liquid metal Rankine cycle powerplants in this analysis were in the reactor and the radiator. The Rankine cycle powerplant employs a fast reactor requiring a large uranium fuel inventory and more stringent safety precautions. The

Brayton cycle reactor concept is a thermal reactor with a slightly larger core volume than the comparable liquid metal cooled fast reactor.

A conical shaped radiator stressed for launch was used in the liquid metal Rankine cycle which had a specific mass ranging from 1.6 to 2.2 kg/kwe. The flat panel radiator used in the Brayton cycle powerplant had a specific mass ranging from .78 to .82 kg/kwe. Since the Brayton cycle powerplant required more radiator area at a given power level and the radiator materials are not the same, these figures cannot be compared directly. However, it is apparent that some savings in radiator mass can be obtained by using a flat panel radiator designed purely as a radiator.

B. Spacecraft Considerations

One of the most costly spacecraft items in terms of mass is the reactor shield. As already pointed out, the use of a fast reactor in the liquid metal Rankine cycle implies a smaller, more compact reactor than a typical thermal reactor such as used in the Brayton cycle. The difference in reactor sizes means a smaller source to be shielded in the Rankine cycle and hence a smaller shield. The greater problems associated with shielding the fast neutron flux from a fast reactor,

however, affect the small size advantage it maintains over the thermal reactor. Although it has not been verified in this analysis, it is felt that the resultant shield mass of a thermal reactor would be less than that for a fast reactor of identical geometry.

Because of the location of the power conversion equipment in the Brayton cycle spacecraft, the resultant reactor shield is heavier than the minimum required. This is a result of the allowable dose at the power conversion equipment, with the center of the equipment approximately three meters aft of the reactor, being more critical in the shielding calculation than the payload dose. With a cylindrical or conical shaped radiator, the power conversion equipment can easily be moved aft, inside the radiator, with little consequence and hence lessen the received radiation dose. With the flat plate radiator design, however, the whole vehicle would have to be extended and this was not done. Hence, if the Brayton cycle reactor shield were sized on the allowable payload dose, its mass would be less than shown in Table IX.

The most critical item in sizing the spacecraft was the required size of the propellant tanks. The selection of the four tanks dictated a total vehicle diameter equal to that of the Saturn V second stage. The large mass of these tanks

makes them the greatest single influence on the resultant spacecraft specific mass. For the case of 40,000 kg of propellant required, the tank mass is approximately one-third of the total spacecraft mass. No attempt has been made in this report to minimize tank mass or to improve upon the configuration as presented. It is felt, therefore, that this is one of the best areas to investigate in an attempt to reduce the spacecraft specific mass. It is noted, for instance, that the surface area of the shroud surrounding the four tanks in Figure 16 is approximately two-thirds of the total tank surface. Applying the required insulation and meteroid protection to a thin shroud surrounding the tanks, instead of the tanks themselves, might represent a considerable savings in total mass.

One of the most often raised objections to a Brayton cycle space powerplant is the large radiator area required. It was for this reason that a flat plate radiator, requiring the minimum panel area, was initially selected in this study. As a result of the large vehicle diameter required for the propellant tanks for the round trip Mars mission, however, it is evident that there is more than sufficient surface area available for packaging a Brayton cycle conical radiator in a vehicle similar to that depicted in Figure 16 for the liquid metal Rankine cycle. Although this would increase the total

spacecraft mass, the packaging advantages of a conical radiator may well outweigh the small mass increases.

The last area of major significance in the spacecraft design is the thruster and its associated equipment. Much work is being done in the area of thruster development and it is hoped that in the near future more information on actual hardware will be available.

C. Powerplant and Mission Compatibility

The preliminary mission analysis conducted in this report was intended only to determine the magnitude and effect of the principal powerplant parameters on the performance of the selected mission. The final propulsion parameters derived in this report were applied to the preliminary mission analysis to determine which set of parameters produced the minimum mission time. A more rigorous mission analysis using the generated propulsion system parameters should be conducted to verify these results.

The resultant spacecraft specific mass for each of the three power levels, and for each of the two cycles concerned, has been plotted against initial mass in Figure 18. The data from this plot can be used directly to interpret the mission analysis graphs, Figures 1 through 4, for the minimum trip time at a given initial mass. For instance, the specific

spacecraft mass, α_s for 1500 kwe Brayton cycle at an initial mass of 45,000 kg is approximately $\alpha_s = 9.5$ from Figure 18. Using this α_s in Figure 2, it can be seen that the total trip time for the round trip to Mars can be accomplished in 550 days when commencing with Earth escape velocity and terminating in low Earth orbit. As another example, the α_s for a 1500 kwe spacecraft at an initial mass of 65,000 kg is approximately $\alpha_s = 10.4$. From Figure 4, at these values, the total trip time becomes 600 days when commencing from and terminating in low Earth orbit.

It is apparent when applying the data from Figure 18 to the mission analysis graphs, that the 1500 kwe spacecraft is significantly better over the ranges of spacecraft specific mass and initial mass plotted in Figures 1 to 4. This immediately suggests that a 2000 kwe spacecraft might be even better, particularly at slightly higher values of initial mass.

A significant fact is the effect of small variations of spacecraft specific mass on total trip time. In the two examples previously stated, the use of the specific masses for the Rankine cycle spacecraft, approximately 1 kg/kwe greater, would result in a total trip time increase of only 20 days. Hence, the criterion dictating minimum mass in component selection might not always be the best solution for the mission

Nuclear Turboelectric Spacecraft Mass
vs
Initial Mass
Earth-Mars Round Trip Mission

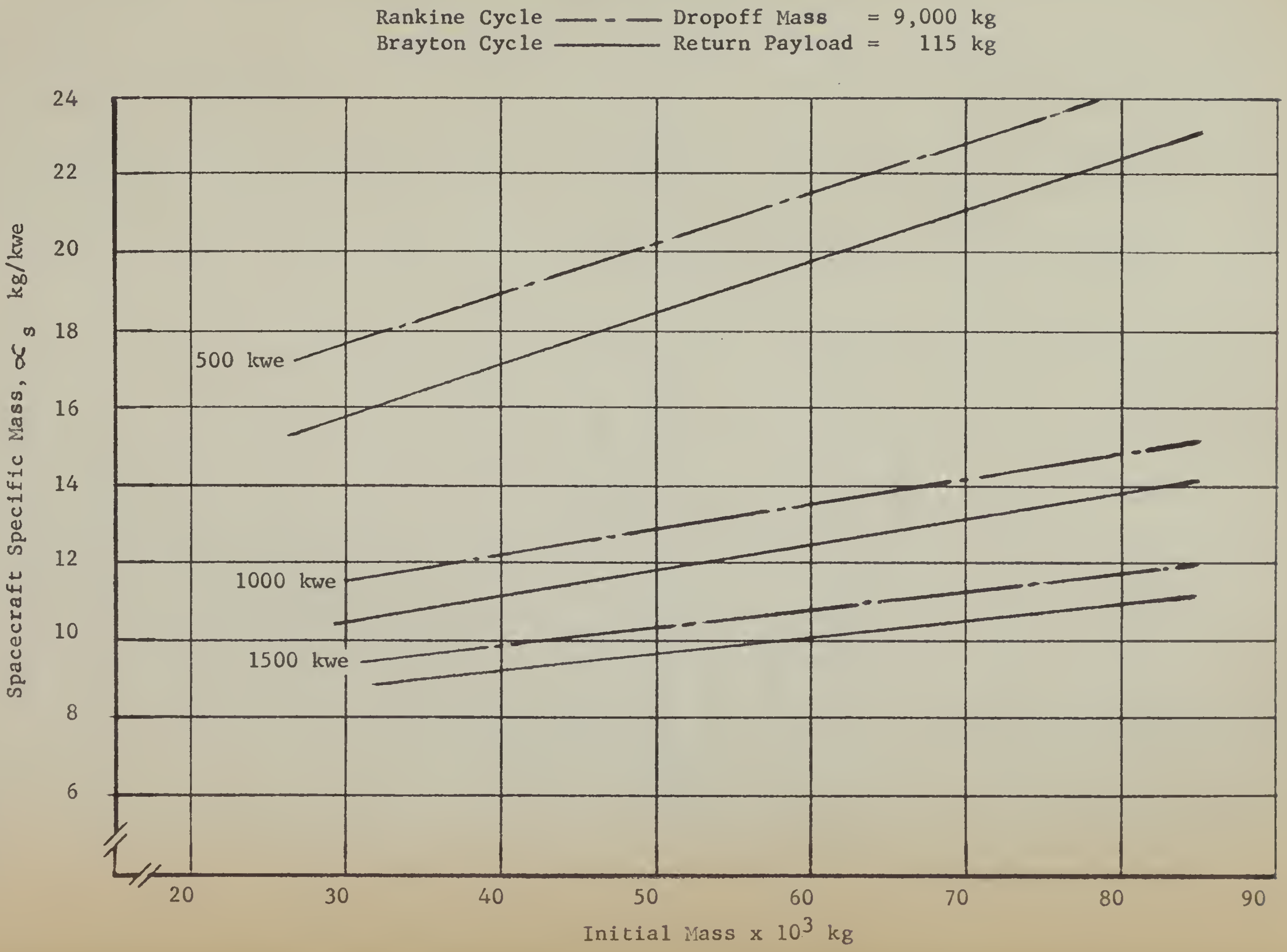

FIGURE 18

being considered. It is felt that this fact adds strength to the case for considering a conical radiator for the Brayton cycle spacecraft as conceived in this analysis. Also, it is obvious that the final difference in spacecraft specific mass, in terms of total trip time, between the liquid metal Rankine cycle and the Brayton cycle spacecraft as depicted herein is small for the higher power levels.

To improve the spacecraft performance at a specific power level, the items inherent to the spacecraft such as the shield, tanks and thrusters are considered the most important because of their large mass. It is felt that there is much better probability of mass reduction in this area than in further consideration of the powerplants themselves.

VI. CONCLUSIONS AND RECOMMENDATIONS

The Brayton cycle nuclear turboelectric space powerplant with a 1665°K turbine inlet temperature has a powerplant specific mass which compares very favorably with that of the liquid metal Rankine cycle powerplant. In addition, the inert gas working fluid in the Brayton cycle has the following advantages: (a) the material development required to raise the turbine inlet temperature and obtain better powerplant performance appears easier to accomplish than similar material development of liquid metal structural and containment materials, (b) an inert gas is definitely superior from the standpoint of starting considerations, and (c) the compatibility of an inert gas with all structural materials will be of measurable assistance in increasing component reliability. In view of these considerations, it is concluded that the Brayton cycle nuclear turboelectric space powerplant has a higher development potential than the liquid metal Rankine cycle space powerplant.

For spacecraft of the size considered in this analysis, thermal reactors are considered more advantageous than fast reactors for use as the energy source in nuclearelectric space powerplants.

The major spacecraft components represent as much as half of the total spacecraft mass, less the payload and propellant.

Accordingly, the spacecraft components are as great an influence on the overall mission performance as is the nuclear turboelectric powerplant. The major spacecraft component is the propellant tankage, representing almost one-third of the spacecraft specific mass.

Based on the mission analysis considered, the 1500 kwe spacecraft can perform the selected mission in less time than the other vehicles. A change in spacecraft specific mass, for this particular vehicle and mission concept of $\alpha_s = 1$ kg/kwe produces a small change in total trip time of approximately 20 days.

The following specific recommendations are made:

1. More research should be undertaken to develop a high temperature Brayton cycle nuclear turboelectric space powerplant for use in spacecraft propulsion.

2. The advantages and disadvantages of a conical radiator should be more thoroughly investigated for spacecraft of the size considered in this analysis for use with the Brayton cycle space powerplant.

3. A more detailed spacecraft design, with particular emphasis on the reactor shield, propellant tankage and thrusters, should be developed for the unmanned round trip mission to Mars utilizing a 1500 kwe Brayton cycle nuclear turboelectric space powerplant.

4. The relative ability of the 1500 kwe spacecraft to perform the selected mission, at a spacecraft specific mass on the order of α_s = 10 kg/kwe, should be verified by a more rigorous mission analysis.

APPENDIX A: References

1. Mariner II Reports, NASA Facts NF B-9-63.

2. Hearings Before the Committee on Aeronautical and Space Sciences, United States Senate, Part I, March 4, 1964.

3. Loomis, A. A., Some Geological Problems of Mars, JPL 32-400, March 4, 1963.

4. Aviation Week and Space Technology, February 1, 1965, p. 27.

5. Aviation Week and Space Technology, July 13, 1964, p. 48.

6. Annual Summary Report Snap 50/Spur Powerplant System for Period ending 31 December 1963, AiResearch Manufacturing Company, APS-5071-R, 31 January 1964.

7. Richardson, W. P., Investigations of a Hybrid Rocket Powered Unmanned Mars Excursion Vehicle, Senior Thesis, Princeton University, June 1964.

8. Neuman, Temple, W., The Preliminary Design of a Mars Excursion Module, AIAA/NASA Third Manned Space Flight Meeting, November 1964, AIAA Publication CP-10.

9. Handelsman, M., Unpublished Notes, RCA, M&SR, December 9, 1964.

10. Sauer, C. G. and Milbourne, W. G., Optimum Earth to Mars Round Trip Trajectories Utilizing a Low Thrust Power-Limited Propulsion System, CIT 32-376, 29 March 1963.

11. Need for More Accurate Information Sets Planned Landing Back to 1985, Missiles and Rockets, November 30, 1964.

12. Williams, P. M., Solid Core Nuclear Reactor Types for Space Powerplants, Unpublished.

13. Combs, M. A. and Norman, L., Applications of the Brayton Cycle to Nuclear Electric Space Power Systems, AIAA Paper 64-757, September 1964.

14. Larson, J. W., Widmer, T. F. and Coy, E. R., Research on Spacecraft and Powerplant Integration Problems, GE No. 6430892, July 24, 1964.

15. Kovacik, V. P. and Ross, O. P., Performance of Nuclear Electric Propulsion Systems, IAS Report 59-25.

16. Shepherd, L. R., Nuclear Power Sources for Electrical Propulsion, Journal of the British Interplanetary Society, March-April 1964.

17. Klann, J. L. and Kerwin, P. T., A Parametric Exploration of Axial-Flow Turbines for Rancine Cycle Space Powerplants in the Megawatt Range, NASA TN D-2544, December 1964.

18. English, R. E., et al., A 20,000 kw Nuclear Turboelectric Power Supply for Manned Space Vehicle, NASA Memo 2-20-59E, March 1959.

19. Grey, J. and Williams, P. M., Re-examination of Gas-Cycle Nuclear-Electric Space Powerplants, AIAA Journal, vol. 1, no. 12, pp. 2801-2811, December 1963.

20. Annual Summary Report SNAP 50/SPUR Power System, AiResearch Manufacturing Company, APS-5071-R, January 31, 1964.

21. Dannak, J. H., SNAP 50/SPUR Power System Quarterly Progress Report, AiResearch Manufacturing Company, APS-5090-R1, 18 May 1964.

22. Glassman, A. J., Summary of Brayton Analytical Studies for Space-Power System Applications, NASA TN D-2487.

23. Vanaco, M. R., Analytical Comparison of Relative Heat-Transfer Coefficients and Pressure Drops of Inert Gases and their Binary Mixtures, NASA TN D-2677, February 1965.

24. Silverstein, A., Conference on New Technology, NASA SP-5015, 5 January 1964.

25. 100 kw Closed Brayton Cycle Space-Power System Using a Gas-Cooled Nuclear Reactor as the Heat Source, AiResearch Manufacturing Company, APS-5042-R, 3 March 1964.

26. Glassman, A. J., A Look at the Thermodynamic Characteristics of Brayton Cycles for Space Power, AIAA Paper 63-218, 20 January 1963.

27. Arave, R. J., Thermodynamic and Normal Shock Properties of the Inert Gases in Ionization Equilibrium, Boeing Report D2-22291, October 1963.

28. Merkle, T. C., The Nuclear Ramjet Propulsion System, UCRL-5625, 30 June 1959.

29. Glasstone S. and Sesonske, A., Nuclear Reactor Engineering, D. Van Nostrand Company, Inc., 1963.

30. Glassman, A. J., Krebs, R. P. and Fox, T. A., Brayton Cycle Nuclear Space Power Systems and Their Heat-Transfer Components, Paper for Sixth National Heat Transfer Conference, Boston, Massachusetts, 14 August 1963.

31. Callinan, J. P. and Berggren, W. P., Some Radiator Design Criteria for Space Vehicles, Transactions of the ASME, vol. 81c, pp. 237-244, August 1959.

32. Blizzard, E. P. and Abbott, L. S., Reactor Handbook, vol. III, part B, Shielding, Interscience Publishers, 1962.

33. Goldstein, H., Fundamental Aspects of Reactor Shielding, Addison-Wesley Publishing Company, Inc., 1959.

34. Rockwell, T., Reactor Shielding Design Manual, McGraw-Hill Book Company, Inc., 1956.

35. Brun, R. J., et al., Analysis of Liquid-Hydrogen Storage Problems for Unmanned Nuclear-Powered Mars Vehicles, NASA TN D-587, January 1962.

36. Cryogenic Propellant Feed Systems for Electrothermal Engines, NASA CR-60, May 1964.

APPENDIX B: Mars-Earth Communication Link (Ref. 9)

1. The standard transmission formula is given as:

$$P_R = \frac{P_T \, G_T \, A_R}{4 \pi R^2 \, L} \qquad (1)$$

where

P_R = received power, watts

P_T = transmitter power, watts

G_T = transmitting antenna gain

A_R = receiving antenna effective area, sq. ft.

R = range, ft.

L = loss factors

The bit rate for television transmission, after considering trade-offs among cooling equipment weight, bandwidth, and reliability, is estimated to be

$$I = 4 \times 10^7 \text{ bits/sec.} \qquad (2)$$

Using a fairly efficient modulation scheme results in the receiver power per bit/sec being:

$$\frac{P_R}{I} = 2 \, KT_e \text{ watts/bit/sec} \qquad (3)$$

where

K = Boltzmann's constant

T_e = system effective noise temperature, ^{o}K

Therefore, from Eqs. 1, 2, 3:

$$P_T G_T = 1.4 \times 10^{-14} \, TeR^2 L/AR$$

If we assume that the ground station link will be a NASA Deep Space Instrumentation Facility, (DSIF), we can take the antenna diameter as 210 ft., its efficiency as 0.7 and a noise temperature of 20°K.

For the space vehicle antenna, we use the equation:

$$G_T = \frac{4\pi f}{2} A_T = 50 \quad D_T^2$$

where

f = antenna efficiency = 0.5

A_T = antenna area = $\frac{\pi D^2}{4}$ sq. ft.

D_T = antenna diameter, ft.

λ = wavelength = 0.317 ft. (s-band)

Now, Eq. (4) becomes:

$$P_T D_T^2 = 5.6 \times 10^4 R^2 L$$

where R is in astronomical units.

The system loss factor, L, is considered to consist of the following:

Alleviation and other plumbing losses	2 db
Transmitter operation off design peak	1 db
Space antenna painting error......................	1 db (10 ft d
	2 db (20 ft d
Transmission path losses	1 db
Noise temperature fluctuations....................	3 db
Other losses and degradation......................	2 db
	L≈10 db

Using L = 10 db, Eq. (6) becomes:

$$P_T D_T^2 = 560 R^2$$

where

P_T = vehicle transmitter power, kilowatts
D_T = vehicle antenna diameter, feet
R = vehicle distance to Earth, A.V.

APPENDIX C: Preliminary Mission Analysis, Ref. 10

The final and initial mass for each phase of the mission are related by

$$\frac{1}{M_f} = \frac{1}{M_o} - \frac{J_i}{2P_j} \tag{1}$$

as shown in the text. Solving Equation (1) for the initial mass gives

$$M_o = \frac{2P_j M_f}{2P_j - J_{in} M_f} \tag{2}$$

The mission as described in the text can be broken into the following phases

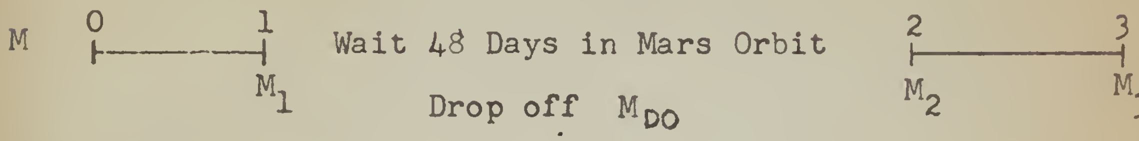

where

0 - 1 is heliocentric transfer to Mars and spirial into low Mars orbit requiring a value of $J_{out} = J_{EM} + J_{sM}$

2 - 3 is spiral out at Mars, heliocentric transfer to Earth and spiral into low Earth orbit requiring a value of $J_{in} = J_{sM} + J_{ME} + J_{sE}$

therefore with

$$M_1 = M_2 + M_{DO} \; ; \quad M_3 = M_s + M_{PL} \tag{3}$$

and applying Equation (2) to each phase

$$M_o = \frac{2P_j M_1}{2P_j - J_{out} M_1} \; ; \; M_2 = \frac{2P_j M_3}{2P_j - J_{in} M_3} = \frac{2P_j (M_S + M_{PL})}{2P_j - J_{in}(M_S + M_{PL})}$$

and

$$M_1 = M_2 + M_{DO} = \frac{2P_j (M_S + M_{PL})}{2P_j - J_{in}(M_S + M_{PL})} + M_{DO}$$

thus

$$M_o = \frac{2P_j \left[\dfrac{2P_j (M_S + M_{PL})}{2P_j - J_{in} (M_S + M_{PL})} + M_{DO} \right]}{2P_j - J_{out} \left[\dfrac{2P_j (M_S + M_{PL})}{2P_j - J_{in}(M_S + M_{PL})} + M_{DO} \right]}$$

or dividing by $2P_j$

$$M_o = \frac{\dfrac{M_S + M_{PL}}{1 - \dfrac{J_{in}}{2P_j} (M_s + M_{PL})} + M_{DO}}{1 - \dfrac{J_{out}}{2P_j} \left[\dfrac{M_S + M_{PL}}{1 - \dfrac{J_{in}}{2P_j} (M_S + M_{PL})} + M_{DO} \right]}$$

APPENDIX D: Modified One Group-Age Diffusion Critical Mass Determination

The age diffusion critical equation for a bare reactor is given as,

$$\frac{k_\infty e^{-B_c^2 \tau}}{1 + L^2 B_c^2} = 1 \tag{1}$$

From one group theory the following relation exist;

$$k = \eta \epsilon p f \quad \text{and} \quad \eta = \nu \frac{\Sigma_f}{\Sigma_a} \tag{2}$$

Since a reactor with fully-enriched fuel is considered, for U_{235}, $\epsilon p \approx 1$ and allowing for fuel burnup, $k_{eff} > 1$. Therefore, combining equation (1) and (2) we have:

$$k_{eff} = \frac{\nu \Sigma_f f e^{-B_c^2 \tau}}{\Sigma_a (1 + L^2 B_c^2)} \tag{3}$$

From Table 4-2, Ref. 30, the expression for buckling for a finite cyclinder is

$$B_c^2 = \left(\frac{2.405}{R}\right)^2 + \left(\frac{\pi}{H}\right)^2 \tag{4}$$

The diffusion length, L, is given by the expression,

$$L = \frac{1}{3 \Sigma_s \Sigma_a} \tag{5}$$

The Fermi age, τ, is approximated by,

$$\tau = \frac{\tau_{BeO}}{\text{Volume fraction of BeO}}$$

The macroscopic cross sections are defined as

$$\begin{aligned} \Sigma_a &= N_{UO_2}\ 0_{a_{UO_2}} \\ \Sigma_s &= N_{UO_2}\ 0_{s_{UO_2}} + N_{BeO}\ 0_{s_{BeO}} \\ \Sigma_f &= N_{UO_2}\ 0_{f_{UO_2}} \end{aligned} \qquad (6)$$

Substituting equations (5) and (6) into (3)

$$K_{eff} = \frac{\gamma_f \left(N_{UO_2}\ \sigma_{f_{UO_2}}\right)\ e^{-B_c^2}}{\left(N_{UO_2}\ \sigma_{a_{UO_2}}\right)\left[\frac{B_c^2}{1 + 3N_{UO_2}\ \sigma_{s_{UO_2}} + \sigma_{s_{BeO}}\ \sigma_{a_{UO_2}}}\right]} \qquad (7)$$

where all quantities are known or can be determined from the volume density and physical dimensions of the core with the exception of N_{UO_2} , the number of nuclei per unit density of UO_2 , and f , the infinite multiplication factor.

To allow for a relative small amount of fuel burnup, a value of $k_{eff} = 1.2$ was used. Beginning with the assumption that $f \approx 1$, an iterative solution of equation (7) was performed for the final value of N_{UO_2} . The required mass or uranium was then determined in kg as follows:

$$M_U = \frac{N_{UO_2}\ (\text{Vol. Core})}{.602 \times 10^{24}} \times 235 \qquad (8)$$

APPENDIX F: Bibliography on Nuclear Space Powerplants of 300 kw and Above

1. Kroeger, H. R., The Case for a Solar Steam Power System ASTRA Report 846-61, 6 January 1964.

2. English, R. E. et al., A 20,000kw Nuclear Turboelectric Power Supply for Manned Space Vehicles, NASA Memo 2-20-59E, March 1959.

3. Moffin, T. P. and Klag, F. W., Analytical Investigation of Cycle Characteristics for Advanced Turboelectric Space Power Systems, NASA TN D-472, October 1960.

4. Powell, R. W., Snap 8 Turboelectric Nuclear Space Power System Including Component Tests, Corrosion Program and Status of Systems, AIAA 64-758.

5. Fimple, W. R. and Edelbaum, T. N., Applications of Snap 50 Class Powerplants to Selected Unmanned Electric Propulsion Missions, AIAA Paper 64-494, July 1964.

6. Beal, R. J. et al., The Electric Space Cruiser for High Energy Missions, JPL TR-32-404, 8 June 1963.

7. A Summary Comparison of Typical Potassium and ASTRA Concept Steam Power Systems, (Layton's office).

8. Systems for Nuclear Auxiliary Power - An Evaluation USAEC T10-20079, January 1963.

9. Davis, N. L., The Future of the Rankine Cycle in Space, Nucleonics, Vol. 22, No. 3, March 1963.

10. Kroeger, H. R. and Grey, J., A Steam-Cycle Powerplant for High Power Communications Satellites, ASME Paper, November 1963.

11. Fraas, A. P., The MPRE - A boiling Potassium Reactor System, AIAA Paper 64-763.

12. d'Arcy, R. J. and Sinko, G. C., Unmanned Electric Propulsion Mission Capabilities of Snap 50 Powerplant, AEC PWAC 447, 22 October 1964.

13. Shipper, L. et al., Advanced 1 Megawatt Space Power Plant Study, AIAA 63-270, Rocketdyne 17 June 1963.

14. Zipkin, M. A., Large Turbo-Nuclear Space Power Systems, pp. 201-261, Advanced Propulsion Concepts, Proceedings of 3rd Symposium, Vol. I, General Electric 1962.

15. Parker, K. D. and Stone, R. A., SPUR High Temperature Space Radiators in Power Systems for Space Flight, Vol. II of Progress in Astronautics and Aeronautics, Ai-Research.

16. Pinsley, E. A., and Gobetz, F. W., Performance of Electrical Propulsion Systems Using Snap 8 Power Supplies, United Aircraft Report B110020-2.

17. Annual Summary Report SNAP 50/Spur Powerplant System for Period ending 31 December 1965, AiResearch Manufacturing Company, APS-5071-R, 31 January 1964.

18. Larson, J. W., Research on Spacecraft and Powerplant Integration Problems, 3rd and 4th Quarterly Reports, GE 64 50 700, 26 April 1964.

19. Stone, R. A., Radiators for Snap 50/Spur, Tech. Report AFAPL-TR-64-113, AiResearch, March 1965.

20. Dannan, J. H., Preliminary Design of a Static Frequency Converter for Snap 50/Spur, AiResearch APS-5128-R, 16 December 1964.

21. Berenson, P. J., Forced Convection Vaporization of Potassium in a Single Tube, APL TDR 64-115, November 1964.

22. Berenson, P. J., Flow Stability is a Multitube Forced Convection Vaporizer, AiResearch L-9448, 21 April 1964.

23. Rackley, R. A. and Gruntz, R. D., Snap 50/Spur Power Conversion System Objectives, Current Status and Lunar Applications, AiResearch APS-5136-R, 5 February 1965.

24. Meis, C. J. and Shapiro, A., Thermodynamic Properties of Alkali Metal Vapors and Mercury, 2nd Revision, GE R60 FPO 358-A, 9 November 1960.

25. Widmer, T. F., Research on Spacecraft and Powerplant Integration Problems, 1st Quarterly Report, GE 63 50 760, 20 June 1963.

26. Burdi, G. F., SNAP Technology Handbook, vol. I, Liquid Metals, AEC NAA-SR-8617.

27. Kumpitsch, R. C. et al., Study of Liquid Metal NaK-77 for Application in Flight Control Systems, AF Systems Command, ASD-TDR-62-597.

28. Dannak, J. H., Snap 50/Spur Power System Quarterly Progress Report, AiResearch, APS-5090-R1.

29. Straugh, R. I. and Chalfant, A. I., High Temperature Technology for the Snap 50/Spur Nuclear Electric Space Powerplant, SAE Paper 861E, 30 April 1964.

30. Glassman, A. J., Analytic Investigation of Recirculation Pump and Radiator-Area Requirements for Flash Vaporization in a Turboelectric Space Power System, NASA TN-D-1283, July 1962.

31. Larson, J. W., Research on Spacecraft and Powerplant Integration Problems, Topical Report GE 64SD892, 29 July 1964.

32. Robinson, R. L. and Raessler, W. U., Long Duration Space Power System Comparison, SAE Paper 8678, 30 April 1964.

33. Coombs, M. G. and Norman, L., Applications of the Brayton Cycle to Nuclear Electric Space Power Systems, AIAA Paper 64-757, September 1964.

34. Stewart, W. L. et al., The Brayton Cycle for Space Power, SAE Paper 1963.

35. 100kw Closed Brayton Cycle Space Power System Using a Gas-Cooled Nuclear Reactor as the Heat Source, AiResearch APS-5042-R, 3 March 1964.

36. Glassman, A. J., Summary of Brayton Cycle Analytical Studies for Space Power System Applications, NASA TN D-2487, September 1964.

37. Shepherd, L. R., Nuclear Power Sources for Electrical Propulsion, Journal of the British Interplanetary Society, March-April 1964.

38. Snyder, H. J., et al., A Spacepower Conversion System Utilizing the Brayton Cycle and a Direct Coupled Nuclear Reactor, AIAA 64-454, Aerojet and Ai-Research.

39. Grey, J., A Research Program on Gas-Phase Heat Transfer Augmentation, Princeton University, 1 March 1965.

40. McBride, B. J. et al., Thermodynamic Properties to 6000°K for 210 Substances, NASA SP-3000, 1963.

41. Arane, R. J., Thermodynamic and Normal Shock Properties of the Inert Gases in Ionization Equilibrium, Boeing D2-22291, October 1963.

42. Vanes, M. R., Analytical Comparison of Relative Heat Transfer Coefficients and Pressure Drops of Inert Gases and their Binary Mixtures, NASA TN D-2677.

43. Glassman, A. J., A Look at the Thermodynamic Characteristics of Brayton Cycles for Space Power, AIAA Paper 63-218.

44. Lieblein, G., Special Requirements on Power Generation Systems for Electric Propulsion, Proceedings of the NASA-University Conference on the Science and Technology of Space Exploration, vol. 2, pp. 157, November 1962.

45. Pedersen, E. S., Nuclear Energy in Space, Prentice Hall, Inc., 1964.

46. King, C. D., Nuclear Power Systems, Macmillan Company, New York, 1964.

47. Thorpe, B. J. and Arker, A. J., Nuclear Electric Power for Manned Space Stations, AIAA Paper 64-713.

48. Volkoff, J. J., Protection Requirements for the Assistance of Meteroid Penetration Damage of Interplanetary Spacecraft Systems, JPL CIT 32-410, July 1964.

49. Cooley, W. C., Advanced Nuclear and Solar Propulsion Systems, Advances in Space Science and Technology.

50. Granich, S. et al., A Nuclear Electric Propulsion System for Manned Interplanetary Missions, Douglas Aircraft Engr. Paper 1787.

51. Davis, J. P., Selection of Power Requirements for Nuclear-Electric Spacecraft Missions, MPL CIT 32-114, 24 May 1961.

52. Grey, J., Williams, P. M., Re Examination of Gas-Cycle Nuclear-Electric Space Powerplants.

53. Grey, J., Williams, P. M., Evaluation of High Performance Nuclear-Electric Cycles for Space Power, RCA R-2, 30 November 1964.

54. Grey, J. Williams, P. M., Analysis of Gas Cycle and Hybrid Nuclear Electric Space Power Systems, October 1963.

55. Cohen and Bordner, An Engineering Evaluation of Advanced Nuclear Thermionic Space Powerplants, AIAA 64-766.

56. Beale, R. J., Nuclear Electric Spacecraft Concepts for Unmanned Planetary Exploration, CIT 32-303, June 1962.

57. Zucrow, M., Space Propulsion Engines - Their Characteristics and Problems, pp. 409-436 of American Scientist, September 1962.

58. Grey, J. et al., Space Nuclear-Electric Systems for Manned Interplanetary Flight Missions, 20 September 1962.

59. Cohen, A. D. and Beers, L. S., Mars Capabilities for Electrical, Nuclear and Chemical Propulsion Systems, IAS 62-120, General Electric.

60. Davidson, E. H., Winslow, P. C., Space Debris Hazard Evaluation, NASA TN D-1105, December 1961.

61. Vanaco, M. R., Glassman, A. J., Analytical Investigation of the Radiator Area Characteristics of Out-of-Pile Thermionic Gas Cycle Space Power Systems, NASA TN D-2429, August 1964.

62. Kovacik, V. P., and Ross, D. P., Performance of Nuclear Electric Propulsion Systems, IAS Report 59-25.

63. Janicke, M. J., Vapor Cycle Coolant Requirements for Nuclear Space Power Plants, AEC ANL-6857, March 1964.

64. Glassman, A. J., Kochs, R. P. and Fox, T. A., Brayton Cycle Nuclear Space Power Systems and their Heat Transfer Components, Paper for Heat Transfer Conference, Boston, Mass., 14 August 1963.

65. Kays, W. M., Basic Heat Transfer and Flow Friction Design Data for Gas Flow in Circular and Rectangular Cylindrical Tube Heat Exchangers, Stanford University TR 14.

66. Kays, W. M. and Lo, R. K., Basic Heat Transfer and Flow Friction Design Data for Gas Flow Normal Banks to Staggered Tubes - Use of a Transient Technique, Stanford University TR 15.

67. Rubin, I. and Imber, M., Optimization Study of Space Radiators, AIAA Journal, vol. 2, no. 2, pp. 353, February 1964.

68. Bartas, J. G. and Sellers, W. H., Radiation Fin Effectiveness, Transactions of ASME, 82c, pp. 73-74, February 1960.

69. Callinan, J. P. and Berggren, W. P., Some Radiator Design Criteria for Space Vehicles, Transactions of ASME, 81c, pp. 237-244, August 1959.

85. Blizard, E. P. and Abbott, L. S., Reactor Handbook, vol. III, part B, Shielding, Intersciences Publishers, 1962.

86. Glasstone, S. and Seconske, A., Nuclear Reactor Engineering, D. Van Nostrand Company, Inc., 1963.

87. Jahn, R. G., Electric Propulsion, American Scientist, Vol. 52, No. 2, June 1964.

88. Richter, R., Equipment and Circuit Conditioning for Plasma, PRC Jet Engine, AIAA Paper 64-678, General Electric.

89. Todd, J. P., et al., The Development of a Regeneratively Cooled 30 kw PRC Jet Engine, AIAA Paper 64-671.

90. Bennett, S., et al., Development of a 3kw Register Jet-AVCO, AIAA Paper 64-672.

91. Toms, R. S., et al., Nuclear Electric Power Requirements for Electric Rockets, AIAA Paper 64-675.

92. Erway, D. D. and Eilenberg, S. L., Power Conditioning, Switching and Controls for Space Propulsion Systems Using Ion Thrusters, AIAA Paper 64-680, 2 September 1964.

93. Kelly, K. T. et al., Corrosion of High Temperature Materials in Alkali Metals, Nucleonics, Vol. 22, No. 3, March 1964.

94. Burkert, H. E., Space Propulsion Materials Data - Appendix to Propulsion Systems Survey.

95. Beckett, C. W., Thermodynamic Propertiesoof Metals, NBS Report 6297, 1 January 1959.

96. Hibben, R. D., Lithium Tests, Aviation Week, 2 November 1964, CANEL.

97. Technical Papers from AIAA 6th Structures and Materials Conference, 7 April 1965.

98. Silverstine, A., NASA Conference on New Technology, Lewis Research Center, NASA SP-5015, 5 June 1964.

99. Darwin, G. E. and Buddery, J. H., Beryllium, Butterworths Scientific Publications, London, 1960.

100. Hodge, W., Beryllium for Structural Applications, Battelle Memorial Institute, DMIC Report 168, 18 May 1962.

101. Elliot, D. J., et al., Investigation of Liquid MHD Power Conversion, AIAA Paper 64-760.

102. Loomis, A. A., Some Geological Problems of Mars, JPL CIT TR 32-400, March 1963.

103. Cavicchi, R. H., and Miser, J. W., Determination of Nuclear Rocket Power Levels for Unmanned Mars Vehicle Starting from Orbit About Earth, NASA TN D-474, January 1962, Lewis Research Center.

104. Brun, R. J., et al., Analysis of Liquid-Hydrogen Storage Problems for Unmanned Nuclear-Powered Mars Vehicles, NASA TN D-587, January 1962, Lewis Research Center.

105. Peterson, E. L., Maintainability Design Requirements for Future Space Systems, AIAA Paper 65-267, 23 April 1965.

106. May, C. B., Maintenance in a Weightless Environment, AIAA Paper 65-257, 23 April 1965.

107. Mueller, G. E., Launch Vehicle Technology, AIAA Paper 64-527, 2 July 1964.

108. Sandler, G. H. System Reliability Engineering, Prentice-Hall, 1963.

109. NASA Manned Mars Exploration, Need for More Accurate Information Sets Planned Landing Back to 1985, Missiles and Rockets, pp. 69-73, 30 November 1964.

110. Steele, A. J. and Planck, H. F., Vehicle Design Considerations, IAS Paper 63-69, 22 January 1963.

111. Fowle, A. A. et. al., Cryogenic Propellant Feed Systems for Electro-thermal Engines, NASA CR-60, May 1964.

112. Olivier, J. P. and Dempster, W. E., Orbital Storage of Liquid Hydrogen, NASA TN- D-559, August 1961.

113. M , E. J., The Effect of Firm Definition of the Mars Atmosphere on the Payload Capability of Advanced Martian Landers, AIAA Paper 65-22.

114. Speiser, E. W., Performance of Nuclear Electric Propulsion Systems in Space Explorations, JPL CIT TN 32-159, December 1961.

115. Stearns, J. W., Electrical Propulsion Requirements for Planetary and Interplanetary Spacecraft, JPL CIT 32-403, March 1963.

116. Melbourne, W. G., Interplanetary Trajectory Optimization with Power-Limited Propulsion Systems, CIT 32-173, 26 February 1962.

117. Melbourne, W. G., Saner, C. G., Optimum Interplanetary Rendezvous Trajectories with Power-Limited Vehicles, CIT 32-226, 15 October 1962.

118. Melbourne, W. G., Saner, C. G., Payload Optimization for Power-Limited Vehicles, ARS 2370-62, 14 March 1962.

119. Melbourne, W. G., and Saner, C. G., Payload Optimization for Power-Limited Vehicles, CIT 32-250, 9 April 1962.

120. Moeckel, W. E., Fast Interplanetary Missions with Low-Thrust Propulsion Systems, NASA TR-79, 1961.

121. NASA Authorizations for Fiscal Year 1965, Part I, 4 March 1964.

122. Spencer, D. F., et al., Nuclear Electric Spacecraft for Unmanned Planetary and Interplanetary Missions, CIT 32-281, 25 April 1962.

123. Project Beagle Mars Mission Proposed, Aviation Week and Space Technology, 13 July 1964.

124. Rossa, L. C., A Parametric Study of Constant Thrust, Electrically Propelled Mars and Venus Orbiting Probes, NASA TN D-2154, October 1964.

125. Stafford, W. H., et al., Parametric Performance Analysis for Interplanetary Missions Utilizing First Generation Nuclear Stages, NASA TN D-2160, MSFC, October 1964.

126. Mackay, J. S., Preliminary Analysis of Manner Mars Mission Using Electric Propulsion Systems, AIAA 64-498, 29 June 1964.

127. Sauer, C. G., and Melbourne, W. G., Optimum Earth to Mars Roundtrip Trajectories Utilizing a Low-Thrust Power-Limited Propulsion System, CIT 32-376, 29 March 1963.

128. Cohen, A. D. and Beers, L. S., Mars Capabilities for Electrical Nuclear and Chemical Propulsion Systems, IAS Paper No. 62-120, June 1962.

129. Widmer, T. F. and Brown, H., Application of Nuclear Electric Propulsion to Advanced Scientific Missions, AIAA Paper No. 64-714, September 1964.

130. Scientists Testimony on Space Goals before the Committee on Aeronautical and Space Sciences, United States Senate, 10 June 1963.

131. Pickering, W. H., Space Programs Summary, No. 37-22, Vol. VI, CIT JPL, 31 August 1963.

132. Hanel, R. A., et al., Experiments from a Small Probe which Enters the Atmosphere of Mars, NASA TN D-1899, December 1963.

133. Newman, T. W., The Preliminary Design of a Mars Excursion Module, AIAA/NASA CP-10, 4 November 1964.

134. Dixon, F. P., An Early Manned Mars Landing Mission Using the Mars Excursion Module, AIAA/NASA CP-10, 4 November 1964.

135. Item pp. 27, Aviation Week and Space Technology, 1 February 1965.

136. Richardson, W. P., Investigation of a Hybrid Rocket Powered Unmanned Mars Excursion Vehicle, Princeton Senior Thesis, June 1964.